Contrasting seasonal changes in total and intense precipitation in the European Alps from 1903 to 2010

Ménégoz, Martin[1], Valla, Evgenia[1], Jourdain, Nicolas. C.[1], Blanchet, Juliette[1], Beaumet, Julien[1], Wilhelm, Bruno[1], Gallée, Hubert[1], Fettweis, Xavier[2], Morin, Samuel[3], Anquetin, Sandrine[1]

1 CNRS, Université Grenoble Alpes, Institut de Géosciences de l'Environnement (IGE), 38000 Grenoble, France
2 F.R.S.-FNRS, Laboratory of Climatology, Department of Geography, University of Liège, 4000 Liège, Belgium
3 Univ. Grenoble Alpes, Université de Toulouse, Météo-France, CNRS, CNRM, Centre d'Études de la Neige, 38000 Grenoble, France

Abstract

Changes of precipitation over the European Alps are investigated with the regional climate model MAR applied with a 7-km resolution over the period 1903-2010 using the reanalysis ERA-20C as forcing. A comparison with several observational datasets demonstrates that the model is able to reproduce the climatology as well as both the inter-annual variability and the seasonal cycle of precipitation over the European Alps. The relatively high resolution allows to estimate precipitation at high elevations. The vertical gradient of precipitation simulated by MAR over the European Alps reaches 33% km^{-1} (1.21 mm day^{-1} km^{-1}) in summer and 38% km^{-1} (1.15 mm day^{-1} km^{-1}) in winter, on average over 1971-2008 and shows a large spatial variability. A significant (p-value<0.05) increase in mean winter precipitation is simulated in the North Western Alps over 1903-2010, with changes typically reaching 20 to 40% per century. This increase is mainly explained by a stronger simple daily intensity index (SDII) and is associated with less frequent but longer wet spells. A general drying is found in summer over the same period, exceeding 20 to 30% per century in the Western plains and 40 to 50% per century in the Southern plains surrounding the Alps, but remaining much smaller (<10%) and not significant above 1500 m.asl. Below this level, the summer drying is explained by a reduction of the number of wet days, reaching 20% per century over the Northwestern part of the Alps and 30 to 50% per century in the Southern part of the Alps. It is associated with shorter although more frequent wet spells. The centennial trends are modulated over the last decades, with the drying occuring in the plains in winter affecting also high altitude areas during this season and with a positive trend of autumn precipitation occurring only over the last decades all over the Alps. Maximum daily precipitation index (Rx1day) takes its highest values in autumn in both the Western and the Eastern parts of the Southern Alps, locally reaching 50 to 70 $mm.day^{-1}$ on average over 1903-2010. Centennial maxima up to 250 to 300 $mm.day^{-1}$ are simulated in the Southern Alps, in France and Italy, as well as in the Ticino valley in Switzerland. Over 1903-2010, seasonal Rx1day shows a general and significant increase at the annual timescale and also during the four seasons, reaching local values between 20% and 40% per century over large parts of the Alps and the Apennines. Trends of Rx1day are significant (p-value<0.05) only when considering long time series, typically 50 to 80 years depending on the area considered. Some of these trends are nonetheless significant when computed over 1970-2010, suggesting a recent acceleration of the increase in extreme precipitation, whereas earlier periods with strong precipitation also occurred, in particular during the 1950s/1960s.

1. Introduction

The European Alps are often considered as the "water tower" of continental Europe (Beniston et al., 2018), hosting the headwaters of several major European rivers, such as the Rhine, the Danube, the Po, and the Rhône Rivers. Similar to other mountain regions, this stems from both enhanced precipitation rates compared to surrounding lowlands, and by the specific role played by glaciers and the mountain snow cover in regulating the local and regional hydrological cycle (Wanner et al., 1997, Viviroli et al., 2008; 2019). The high population density and the presence of strong slopes make these areas particularly prone to natural hazards such as landslides, floods and avalanches, which are strongly connected to meteorological conditions (e.g. Beniston M., 2006; Raymond et al., 2019; Evin et al., 2019). There is widespread scientific evidence that significant atmospheric warming has occurred and is projected to occur in the European Alps, as a response to anthropogenic forcing (Hock et al., 2019). This warming is estimated to 1.2°C per century over the 20th century (Auer et al., 2007), which is twice as large as global rates (Brunetti et al., 2009; Gobiet et al., 2014). This warming strenghtened over the last decades, with values exceeding 0.3°C per decade (Rottler et al., 2019). Precipitation changes are more difficult to detect because of (i) the difficulty to observe and simulate this variable in particular over mountainous areas, (ii) their dependance to the large climate internal variability and (iii) the spatial heterogeneity peculiar to complex topography areas.

The longest time series of observed precipitation in the European Alps are available in Switzerland and Italy, with station data that have been homogenized over the last 100 to 150 years (i.e starting from 1900 and even before; Schmidli et al., 2002; Brugnara and Maugeri, 2019). Such a long record is useful to investigate precipitation changes, but station data need to be considered carefully, because the spatio-temporal heterogeneity of the data availability might be a cause of spurious trends (e.g. Masson and Frei, 2016). Interpolation of station data can be used to produce gridded products, commonly used to investigate climate variability. For example, S2M (Durand et al., 2009) and SPAZM (Gottardi et al., 2009; 2012) are two reanalysis covering the French Alps, HISTALP (Auer et al., 2007) and EURO4M (Isotta et al., 2014) are a reconstruction of the climate of the European Alps, and E-OBS is a dataset commonly used for model verification over Europe (Cornes et al., 2018). General Circulation Models (GCMs) are also widely used to investigate climate change processes and trends. However, their coarse resolution precludes accurate simulations of small scale processes typical of mountainous areas, such as those inducing the spatial heterogeneity of precipitation and snow cover. It is therefore difficult to study the Alpine climate variability with GCMs (Zubler et al., 2015). Due to their finer resolution (~25 to 1 km) and their more detailed parametrization for physical processes (e.g. precipitation microphysics, surface snow scheme), that can be developed and tuned specifically considering regional geographical features, Regional Climate Models (RCMs) are more adapted to simulate the mountainous climate and can be used to dynamically downscale global climate model or global reanalyses. They have been widely used to simulate the climate in mountainous areas, and in particular temperature (Smiatek et al., 2016), daily and sub-daily precipitation events (Torma et al., 2015; Pieri et al., 2015), precipitation trends (Giorgi et al.,

2016) and snow cover (Steger et al., 2013). A fine resolution is critical to simulate precipitation correctly. Increasing the resolution from 0.44° to 0.11°, Fantini et al. (2018) demonstrated that a RCM better captures the spatial pattern and the seasonal cycle of precipitation as well as its daily intensities and statistics. The improvement of the model performances allows currently to run RCMs at high resolution, typically 1 to 5 km, in non-hydrostatic configurations, resolving the convective processes, and allowing an accurate description of the snow cover in mountainous areas (e.g. Ban et al., 2014, 2015; Luthi et al., 2019; Vionnet et al., 2019). Such configuration is however challenging to run over more than one to two decades due to computational costs.

Internal climate variability in the North Atlantic basin induces large seasonal to multi-decadal variability of precipitation over Europe (Qasmi et al., 2017; Dell'Aquila et al., 2018; Brugnara and Maugeri, 2019). In the European Alps, higher interannual variability is observed in the Southern compared to the Northern Alpine areas (Efthymiadis et al., 2007). Seasonally, higher interannual variability in winter and autumn compared to other seasons has been reported in this area (Brunetti et al, 2009; Bartolini et al, 2009). Over the last decades, precipitation rates have been declining for any period of the year in the mediterranean area (Giorgi et al., 2008; Mariotti et al., 2015), a signal partly attributed to anthropogenic forcings (Hoerling et al., 2012) and associated with a significant surface drying (Douville et al., 2017). Precipitation trends during the last century are more contrasted over the Alps, with a decrease in the Southeastern Alps consistent with the drying of the mediterranean area (Schmidli et al., 2002; Auer et al., 2007; Brugnara and Maugeri, 2019) and an increase in the annual precipitation in the North Western Alps, mainly driven by a positive and significant trend in winter and at high elevation (Masson and Frei, 2014; 2016). Napoli et al. (2019) suggested that the contrasted trends of precipitation between high mountains and lowlands over the last decades is explained by the aerosol forcing that cools the atmosphere mainly at low elevations since the air quality is better at high elevations. Precipitation trends show also strong seasonal contrasts in the Alps (Pavan et al., 2019). In addition, precipitation trends emerge from the natural variability only when considering long time series, typically one century (Schmidli et al., 2002). This result is consistent with previous studies claiming that precipitation rates did not show any significant trend in the Alps when considering shorter periods, as found in Durand et al. (2009) in the French Alps over the period 1958-2002.

Dry spells did not show any clear tendency over the last century in the Alps (Schmidli and Frei, 2005; Brugnara and Maugeri, 2019), whereas the length of dry episodes increased in the Mediterranean area (Kuglitsch et al. 2010). On the other hand, Schmidli and Frei (2005) highlighted contrasting seasonal trends of the wet spell duration in the Swiss Alps, with a lengthening in winter and a shortening in summer. Using 104 rain gauge stations in Switzerland, Schmidli and Frei (2005) found an increase of the high quantiles of precipitation by 10% to 30% over 1901-2000, a result evidencing an increase of extreme precipitation in this area, that they relate to global climate change. This finding has been supported by Scherrer et al. (2016), suggesting an increase of both the intensity and the frequency of heavy precipitation events in Switzerland. The intensity of extreme precipitation is often expected to follow a Clausius-

Clapeyron (CC) relationship with temperature changes, with a scaling rate surrounding 7% $°C^{-1}$ (Trenberth et al., 2003). However, different values of CC scaling rates has been reported in the literrature. Focusing on strong precipitation events observed in Switzerland, and regardless their duration, Molnar et al. (2015) reported super-CC scaling rates between 11 and 13% $°C^{-1}$, partly related to an intensification of convection during the last 30 years. Conversely, Ban et al. (2015) found an increase in extreme precipitation events that asymptotically intensifies following the CC relationship when applying a convection-resolving RCM at 2.2 km resolution over the European Alps. Using model data over the last 400 years and over the 21st century, Brönniman et al. (2018) evidenced a limitation of the available moisture in the atmosphere at the seasonal timescale that limits the increase of heavy precipitation during the summer even with strong warming levels. They pointed out a shift of heavy precipitation events from late summer to early summer and early autumn. Considering the annual maximum of daily precipitation (Rx1day), Brugnara and Maugeri (2019) also found an increase of extreme precipitation in Switzerland over 1890–2017, whereas they could not highlight a clear trend of extreme precipitation in Northern Italy, suggesting a non-uniform spatial change of strong precipitation events. The CC scaling rate show a large spatial variability, in particular because atmospheric circulation patterns may drive heterogenous moisture advection (Molnar et al., 2015), and also because of potential limitation of moisture availability at the local scale (Brönniman et al., 2018). Overall, the CC scaling rate depends on the frequency of the precipitation data considered in the calculation, with higher CC scaling rates generally found when considering data with high frequencies (e.g. hourly versus daily).

RCMs are limited-area models that can be forced laterally with atmospheric reanalysis, often available only for the last decades, such as the ECMWF reanalyses ERA40 (1958-2002, Uppala et al., 2004), ERA-Interim (1979-2019, Dee et al., 2011) and ERA5 (1950 onward, Hersbach and Dee, 2016). Recent reanalysis products available for the whole 20th century (e.g. ERA-20C, 1900-2010; Poli et al., 2016) now offer the possibility to apply RCMs over longer periods although such a reanalysis, assimilating few data, is less reliable than reanalysis built on the satellite era. Most of the observational and modeling data used to investigate climate change in the European Alps generally do not combine a daily resolution, a centennial availability and a fine spatial resolution, precluding investigations of changes in mean and extreme precipitation. This strongly limits the possibility to detect precipitation trends, especially when considering the large internal variability that may overwhelm long-term trends. In this study, daily precipitation variability and changes in the European Alps (referred to as the Alps in the rest of the text) are investigated over the period 1903-2010, using observational datasets as well as the regional climate MAR model applied with a resolution of 7 km and driven by the ERA-20C reanalysis. The material and methods, including a description of the model MAR and different observational datasets are described in Section 2. The model outputs are compared with several observational datasets in Section 3. Seasonal and annual trends of precipitation indices are estimated over 1903-2010 in section 4. A discussion associated with the conclusions is presented in Section 5.

2. Material and methods

2.1 The MAR model

In this section we provide a succinct description of the atmospheric regional model MAR (http://mar.cnrs.fr/), developed at ULiège (Belgium) and IGE (Grenoble). A more detailed description can be found in Gallée and Schayes (1994), Gallée (1995) and Gallée et al. (2001, 2005). MAR is a hydrostatic primitive equation model with a vertical coordinate defined as sigma coordinates. The radiative transfer through the atmosphere uses the radiative scheme of the ECMWF reanalysis (Morcrette, 2002). MAR includes a detailed scheme of clouds microphysics with six prognostic equations for specific humidity, cloud droplets concentration, cloud ice crystals (concentration and number), concentration of precipitating snow particles and rain drops. The convective adjustment is parameterised according to Bechtold et al. (2001). MAR is coupled to the one-dimensional land surface scheme SISVAT (Soil Ice Snow Vegetation Atmosphere Transfer, De Ridder and Schayes, 1997; Gallée et al., 2001) that includes a snow multi-layer scheme (Brun et al., 1992) including prognostic equations for temperature, mass, water content and snow properties (dendricity, sphericity and size) as well as an ice module (Lefebre et al., 2003). As pointed out in Messager et al. (2006), the physics of MAR can be adjusted to the region of interest and can be used with relatively high resolutions (40 to 7 km, finer resolutions would not be possible when using the hydrostatic configuration). MAR is a limited area model that offers the advantage to be able to be forced by most of reanalyses (including ERA-20C) or CMIP5/CMIP6 global model outputs. MAR has been first designed for polar regions (Gallée, 1995), i.e. Antarctica (e.g., Gallée et al., 1996; Naithani, J. et al., 2002; Gallée et al., 2013, Amory et al. 2015; Agosta et al. 2019) and Greenland (Fettweis et al., 2017). It has also been applied over tropical regions (Messager et al., 2004) to investigate the precipitation variability (Gallée, 2004). MAR has also been used to simulate the climate at midlatitudes (e.g. Wyard et al., 2016), and in particular to study changes of precipitation over Europe (Doutreloup et al., 2019). It has been applied over various mountainous areas, e.g. Himalaya (Ménégoz et al., 2013), Svalbard (Lang et al., 2015), Kerguelen archipelago (Favier et al., 2016; Verfaillie et al., 2019) and Antarctic peninsula (Datta et al., 2017).

2.2 MAR configuration

We used the version 3.9.0 of the MAR model, which is an open source code available at https://mar.cnrs.fr/. Here, the model has been applied over the European Alps with a domain that extends from 42.8°N to 48.4°N and 2.5°E to 15.2°E and includes 140 x 90 grid points, at 7 km horizontal resolution. This domain covers most of the European Alps, except its most eastern part over Austria and Slovenia. The model physics being affected at the borders by the lateral forcing, a smaller domain is chosen for the analysis, that extends from 43.5°N to 48°N and from 5°E to 13°E, covering the French, Italian and Swiss Alps, as well as a large part of the Austrian mountains (Figure 1a). This configuration is based on 24 levels in the atmosphere, 7 levels in the soil, and the snow cover is described with a number of layers varying from 1 to 20. Here, MAR

is laterally forced with the 6-hourly outputs of the ERA-20C reanalysis and its dynamical and physical schemes are applied with a time step of 60s. ERA-20C is one of the first reanalyses available from 1900 to 2010, assimilating surface pressure and near-surface winds over the ocean and forced by SST reconstructions (Poli et al., 2016). By assimilating a limited number of variables corresponding to those available relatively homogeneously over 1900-2010, the ERA20-C reanalysis is expected to be homogeneous over this period, with a limited risk of including spurious trends. However this reanalysis is probably less accurate than other products assimilating also humidity and temperature in the free troposphere, a weakness that could induce model biases also in regional experiments as evidenced by Fettweis et al. (2017) over Greenland. The coarse resolution of ERA-20C (~125km) does not allow a correct description of the atmospheric variables over mountainous areas, which justifies the use of a regional model with higer resolution and avanced physical parameterisations. MAR has already been successfully tested with the ERA20-C reanalysis as boundary conditions over Europe (Wyard et al., 2017; 2018). After a spin-up of 2 years, the model in general and the surface component in particular are supposed to reach an equilibrium. Therefore, the first two years have been excluded from this analysis that hence focuses on the period 1903-2010.

2.3 Observational datasets

Observational data sets are used in this study for two objectives: first, a comparison between the model outputs and the different precipitation datasets have been conducted over 1971-2008, a period for which all the datasets are available (Section 3). Second, an analysis of the trends of several precipitation indices is described using the MAR experiments and the MeteoSwiss station data available since the beginning of the 20th century (Section 4). In addition to the MeteoSwiss station data, the following datasets have been considered:

HISTALP

The HISTALP ("Historical instrumental climatological surface time series") is the first long-term database of meteorological data collected in the European Alps, initiated in the 1990s (Auer and Bohm, 1994) and completed later on (Auer, et al., 2007). This dataset is available with a monthly resolution for air temperature at 2 meters, surface pressure, precipitation, sunshine duration and cloudiness through two different configurations: a first one including homogenized time series of local measurements, with the first observations available from 1760 for temperature and 1800 for precipitation and a second one provided as a gridded version. The gridded version, used in our study, is available from 1800 to 2014. Originally available at a 1°x1° resolution (Auer et al., 2007), it is now based on a 5min x 5min resolution (http://www.zamg.ac.at/histalp/dataset/grid/five_min.php).

EURO4M-APGD

The Alpine Precipitation Grid Dataset (EURO4M-APGD, Isotta et al., 2014) is a 5kmx5km grid analysis of daily precipitation, extending over the European Alps and covering the period 1971-2008. It is based on rain-gauge networks, encompassing more than 8500 stations from Austria, Croatia, France, Germany, Italy, Slovenia and Switzerland. This dataset was developed in the framework of the European Reanalysis and Observations for Monitoring (EURO4M) initiative and is simply named EURO4M thereafter.

E-OBS

E-OBS is provided by the ECA&D project under the Copernicus Climate Change Service (van den Besselaar et al., 2011). It is a daily gridded dataset over Europe for temperature and precipitation, produced from interpolation of local measurements at two available resolutions: 0.25° and 0.1° (the highest resolution is used in this study). It is available from 1950 and updated each year, and is commonly used for model evaluation (e.g. Guillod et al., 2017). The version 19 of E-OBS offers an estimate of the uncertainty related to the interpolation of local observations by providing a 100-member ensemble for each variable (Cornes et al., 2018).

S2M

The S2M reanalysis combines large scale reanalyses and forecasts with in-situ meteorological observations, including precipitation, in order to provide a hourly reanalysis of meteorological conditions in the French Alps, at the scale of massifs with a typical surface area of 1000 km2 within which meteorological conditions are assumed to be homogenous but vary with elevation by steps of 300 m (Durand et al., 2009). Hence this reanalysis does not use a regular grid but focuses on the elevation depency of meteorological conditions. A recent version of this open-access reanalysis is now described in Vernay et al. (2019).

SPAZM

The SPAZM dataset is a gridded product at a 1km resolution for minimum and maximum daily 2m temperature and daily precipitation in the French Alps, available over the period 1948-2009 and based on the interpolation of a dense network of rain gauges and temperature sensors from Météo-France and the French Company for Electricity (EDF; Gottardi et al., 2009; 2012). This dataset is provided with calibration parameters allowing to reproduce the stream flow observed in the Rhône valley with a hydrological model. These parameters are useful to correct the snowfall rates that are often underestimated in rain gauge measurements. The solid and liquid precipitation has been computed by considering 100% of solid precipitation below 0°C and 100% of liquid precipitation above 2°C, considering daily temperature. A linear relationship for the ratio liquid/solid precipitation has been applied between 0°C and 2°C. Following the calibration suggested by Picouet (2012), we applied a correction factor for solid precipitation of 1.5 in the Northern Alps and 1.3 elsewhere. The Northern Alps are defined here as the areas located north of Grenoble city (45.1885° N) and higher than 1000m asl. This apparently-arbitrary values have been developed and evaluated in the context of hydrological studies (Gouttevin et al., 2017).

An increasing number of climate data based on observational networks, reanalysis product and model experiments covering the European Alps are available, as described in the project EURO4M (Isotta et al., 2014 and http://www.euro4m.eu/datasets.html for recent updates). The number of products in this study has been limited for practical considerations, but obviously, further investigations could be done with other datasets (e.g. ERA5, Hersbach and Dee, 2016; ARCIS Italian observations, Pavan et al., 2019).

2.4 Statistical analysis and indices

Mean and trends for the precipitation indices described in Table 1 are considered in this study, most of them selected from those recommended by the World Meteorological Organization (Peterson et al., 2001; http://etccdi.pacificclimate.org/list_27_indices.shtml). These indices, for which a full description is shown in Table 1, are the Total precipitation amount, annual or seasonal (TP or STP), the number of wet days (WD), the Simple Daily Intensity (SDII, i.e. the amount of precipitation during the days with precipitation), the Maximum daily precipitation (Rx1day), the Mean Number of Wet Spell per season (MNWS) and the Mean Wet Spell Duration (MWSD). When comparing MAR outputs with observational datasets based on a higher resolution (EURO4M, SPAZM), these ones are linearly interpolated onto the MAR grid. The gridded data are based on regular grids, except the S2M data that is provided with a georeferenced polygon describing the location of each massif. Correlation and Root Mean Square Error (RMSE) are computed to investigate the differences between datasets. The linear trends are computed with a linear least-square regression and a two-sided p-value is computed to test if the trends are significantly different from zero (Wald test with a t-distribution of the test statistic). Mean values and normalized trends (in percentage of the averaged values) are computed annually and seasonally for the precipitation rates and indices in the following sections. The seasons are computed by averaging indices over December-January-February (DJF) for winter, March-April-May (MAM) for spring, June-July-August (JJA) for summer, and September-October-November (SON) for autumn.

3. Climatology of the MAR experiment and the observational datasets

3.1 Spatial differences

The Total Precipitation amount (TP) averaged over 1971-2008 simulated with MAR is shown in Figure 1a, with annual mean ranging between 300 and 3000 mm. In a general way, TP is stronger in the Northern than in the Southern Alps as expected due to the drier Mediterranean climate in the South. A comparison between the MAR experiment and the EURO4M reanalysis (Figure 1b) shows a good consistency between these two datasets in the lowlands (i.e. below 500m asl), with positive or negative differences barely exceeding 20% in these areas, except in the Piedmont-Ticino-Lombardy and in some part of the northern Apennines where the model underestimates the strong precipitation rates specific to these medium elevation areas of the Southern Alps. Above 1500m, this difference is larger with precipitation rates 40 to 80% higher

in the MAR experiment than in the EURO4M dataset. Such a difference is significant with respect to the interannual standard deviation of precipitation that generally does not exceed 30% over the domain of application of MAR (Figure A1). The comparison between MAR and SPAZM (Figure 1c) shows similar differences in the lowlands as with EURO4M (~20%), but a better agreement at high elevation, with differences barely exceeding 40%. Pattern correlation between MAR and EURO4M is 0.59 and reaches 0.63 between MAR and SPAZM, suggesting a slightly better spatial consistency between these last two products. The precipitation rates estimated from SPAZM above 1500m asl are also higher in comparison with those provided by EURO4M (Figure 1d, differences ranging between 20% to 80%). As snowfall rates in SPAZM have been adjusted to fit the hydrological balance over the French Alps, this comparison suggests that the high precipitation rates simulated with MAR above 1500m asl may be realistic. Overall, TP simulated with MAR is relatively similar to TP estimated from SPAZM and shows stronger values with respect to EURO4M data over the Alps.

3.2 Vertical gradients

Vertical gradients of TP simulated with MAR are evidenced in Figure 2 (as yearly averages, considering both wet and dry days), including also a comparison with the S2M reanalysis and the MeteoSwiss station data. In the MAR experiment, TP varies from 2 to 4 mm day^{-1} at 500m asl and from 3 to 5 mm day^{-1} at 2500m asl in the Southern Alps, and from 2 to 4 mm day^{-1} at 500m asl and from 3 to 6 mm day^{-1} at 2500m asl in the Northern French Alps. The vertical gradient estimated from the S2M dataset is smaller than those simulated by MAR. The large spread in the scatter plots of Figures 2a-b is explained by the spatial variability of the vertical gradient of precipitation, which is stronger in MAR than in S2M. Based on a comparison with high resolution numerical weather forecast model and glacier mass balance in mountain glaciers in the French Alps, it has been shown that S2M most likely underestimates high elevation winter precipitation (above 2000m asl), which lends credence to the higher gradients simulated by MAR (Vionnet et al., 2019). MAR data are compared to the MeteoSwiss station data in Figure 2c-d. A difference between the two datasets in terms of vertical gradients is found both in winter (14% km^{-1} for the local observations vs 43% km^{-1} in the MAR data) and in summer (12% km^{-1} for the local observations vs 20% km^{-1} in the MAR data). These seasonally contrasted differences suggest a possible underestimation of the precipitation rates estimated from rain gauge measurements in relation with snowfall undercatch issues (Kochendorfer et al., 2017). However, the differences found in summer, i.e. a period with reduced snowfall rates, also suggest an overestimation of the precipitation rates at high elevation in the MAR experiment. Nevertheless, it is difficult to accurately quantify the model biases at high elevation areas because of the scarceness of the observational data above 2000m asl whereas a large number of the MAR grid cells reaches an elevation ranging between 2000m asl and 3000m asl with a spatial resolution of 7km (Figure 2c-d). An underestimation of the precipitation rates in the model versus the station data is also found in summer at intermediate elevation (500m-1500m, Figure 2d). This difference appearing only in summer suggests an inability of the convective model scheme, that could induce too much convective mixing. Overall, the vertical gradient of

precipitation simulated by MAR over the entire domain of application reaches 38% km^{-1} (1.15 mm day-1 km^{-1}) in winter and 33% km^{-1} (1.21 mm day-1 km^{-1}) in summer (Figure 2e-f). Overall, the spatial patterns shown in Figure 2g-h for the MAR experiment and the MeteoSwiss station data suggest that MAR is able to reproduce the seasonal variations of precipitation rates, with large (small) values in summer in the Northeastern (Southwestern) Alps and an opposite pattern in winter.

3.3 Interannual variability and seasonal cycle

The temporal evolution of precipitation and its seasonal cycle over the period 1971-2008 is shown in Figure 3 for three sub-regions defined as the Southern Alps (SA, 43.5°N to 45.5°N and 5°E to 7.5°E), the North Western Alps (NWA, 45.5°N to 47°N and 5°E to 7.5°E) and the Northeastern Alps (NEA, 45.5°N to 48°N and 7.5°E to 13°E), corresponding respectively to the orange, blue and purple boxes in Figure 1a. These boxes have been defined according to the data availability of the products used for comparisons as well as regional climatological conditions: SA is largely affected by the Meditteranean dry conditions, NWA precipitations rates are mainly related to Western low pressure systems, whereas NEA is more typical of a continental climate, with wetter conditions in summer than in winter. Over 1971-2008, precipitation rates estimated from the different datasets (EURO4M, SPAZM, E-OBS, HISTALP) show similar features. They range between 2 and 4 mm day-1 in SA and take higher values in NWA and NEA, varying between 3 and 5 mm day^{-1}. Table 2 includes the interannual correlations between the different datasets, that takes values above 0.8, except for HISTALP that correlates neither with EURO4M nor with MAR. The correlations between MAR and the observational datasets range between 0.84 and 0.89, whereas the correlations among these different datasets systematically exceeds 0.9, even reaching 0.99 and 0.97 for EURO4M versus SPAZM in SA and NWA. Such high correlation is probably due to the rain gauge network used to produce these gridded datasets that is partially common between the two products. Overall these correlation values suggest a correct interannual variability in the MAR experiment, but less realistic than those estimated from the other observational datasets (except HISTALP). The model bias could be related to both model deficiencies and uncertainties in the ERA-20C reanalysis used as boundary conditions. The difference between the MAR experiment and the observational products is similar in all the datasets, with a RMSE ranging between 0.26 and 1.14. RSME computed with HISTALP are comparable to the other ones, evidencing that HISTALP is able to provide an estimation of precipitation similar to the other products, even if the interannual variability is poorly reproduced in this dataset compared to the other ones (low correlation). No clear regional and data-dependent specificity in terms of RMSE is discernable in Table 2. It is worth noting that the uncertainty related to data interpolation in E-OBS (orange dashed lines) encompasses the time series corresponding to the other datasets. Such a large uncertainty is probably related to the low number of observations assimilated in E-OBS over the Alps in comparison with the large number of meteorological stations used to build EURO4M and SPAZM. This points out the large uncertainty of such gridded products in mountainous areas. MAR is closer to SPAZM and EURO4M (smaller RMSE) than to HISTALP and E-OBS (higher RMSE), a finding giving

confidence in the realism of the MAR simulation. The different datasets show specific seasonal cycles of precipitation (Figure 3, bottom), with two maximum values in spring and autumn in SA (Mediterranean climate), one maximum value in summer in NEA (continental climate) and a mix between these two regimes over NWA. Overall, the consistency between the different datasets is better in SA and NEA than over NWA, where more discrepancies among the datasets have been found. The comparison between model experiments and observational datasets gives confidence in the precipitation rates simulated with the MAR model forced here by ERA-20C. Longer simulations are therefore considered in the next section to investigate potential trends over the last century.

4. Precipitation trends in the Alps over 1903-2010

4.1 Mean annual and seasonal precipitation

No significant trend in precipitation rates is identified on average when considering the three Alpine sub-regions shown in Figure 3, a finding that could be explained by the shortness of the time series. The seasonal trends of mean precipitation (STP) are investigated now over longer periods, by considering in Figure 4 the MAR experiment (shaded) and the MeteoSwiss station data (dotted) over 1903-2010 (left) and over 1958-2010 (right). The MeteoSwiss data is used here because it is available over the period covered by the MAR experiment (i.e. from 1903). Over 1903-2010, trends are contrasted both seasonally and altitudinally. In winter, there is a general positive trend in precipitation over the Alps (up to 40% per century), contrasting with a drying simulated in the surrounding plains (~-10% per century), both in the Po plain and in the Rhône valley (Figure 4b). In winter, the MAR experiment is consistent with the local observations showing an increase in precipitation over Switzerland, except in the southern part of this country, where some stations show a drying trend. However, when masking the non significant trends (p-value>0.05, Figure 4a), only the positive trends of precipitation remain over the Alpine mountains, with values ranging between 20 and 40% per century in the Northern French Alps and in the Southwestern Switzerland, at an elevation generally higher than 1500m asl. The MeteoSwiss data shows a significant increase in precipitation at stations located further north in Switzerland, with a magnitude similar to the model values. In summer, a general drying is simulated over the whole model domain (Figure 4h), with values exceeding 40 to 50% per century in the Po and the Rhône valleys. This signal is much less pronounced in the alpine areas located above 1500m asl, where the signal is generally not significant (Figure 4g). The drying is less pronounced over Switzerland in comparison with the Southern Alps. Considering Figure 4h, a drying and even a slight increase in precipitation (<10% per century) is found in the station data over the mountains of Southern Switzerland, whereas a drying is observed in the north of the country (10% to 20% per century). The summer trends locally observed in Switzerland are however barely significant (Figure 4g). Spring and autumn trends show intermediate patterns, with a drying pronounced in the plains, and a slight moistening in the mountainous areas (Figure 4d-e and 4j-k). The trends simulated and observed during spring and autumn are smaller and barely significant, except in the Po plain where a drying is simulated by MAR and in the North of Switzerland where a moistening is significant at some stations (Figure 4d-j). Over the more

recent period (1958-2010; Figure 4c-f-i-l), the only significant signal is the strong drying found in the Po plain (p-value<0.05) in winter-spring-summer, when more heterogeneous trends are found in the mountains at the same time (not significant, p-value>0.05, non-significant trends are not masked in Figure 4c-f-i-l). The main differences between the trends found over 1902-2010 and 1958-2010 are found in winter, when the drying occurring in the Po plain is more pronounced and extends until the high altitude areas during the more recent period (Figure 4b-c). Also, a strong moistening is found in autumn, especially pronounced in the Northwestern flank of the Alps. This signal occurred mainly over the last decades (Figures 4k-l) but it is generally not significant (p-value>0.05, not shown).

The seasonal changes of precipitation simulated with MAR over the Alps are deeply related to the seasonal changes of moisture in the ERA-20C reanalysis used as boundary conditions (Figure 5). The drying occurring in the Po Plain is related to a drying that occured over a large part of the mediterranean area, in particular over the French and the Italian mediterranean coasts that propagate inland especially during the summer, when southwestern winds transport moisture at the East of the continent (Figure 5c). During the winter and the autumn, a moistening over Germany, Benelux and the North of France and Switzerland is related to an increase of western moisture fluxes that bring moisture from the Atlantic, in particular over the Northern flank of the Alps (Figure 5a-d). The coarse resolution of ERA-20C does not allow a fine estimation of the precipitation changes over the Alps, as it can be done with MAR, but conversely, it is shown here that the spatial features of the precipitation changes over the Alps produced with MAR are largely related to the large-scale moisture changes driven by the ERA-20C boundary conditions.

4.2 Wet spells

Changes of the wet spell features are highlighted in Figure 6, showing the centennial summer and winter trends of WD (Figure 6a-b), SDII (Figure 6c-d), MWSD (Figure 6e-f) and MNWS (Figure 6g-h). In winter and over the Alps, the slight increase in WD, ranging between 0 and 10% per century, is slightly contributing to the increase in the STP (Figure 6a), but this one is mainly explained by an increase in SDII by 10 to 30% per century (Figure 6c). These changes are associated with an increase in the MWSD by 10 to 20% per century (Figure 6e). Finally, the winter trend in the MNWS shows a different pattern from the previous ones (Figure 6g), with a consistent decrease over the Northern Alps and in particular over Switzerland, ranging between 10 and 20% per century in both model and observational data. These changes suggest that the precipitation increase found in winter over the Alpine mountains is related to longer, more intense and less frequent wet spells. The agreement between the model and the observations is relatively good in winter. In summer, a large part of the drying is explained by a reduction of WD, reaching 10 to 20% in the north-western flank of the Alps, and exceeding 40 to 50% per century in the Southeastern Alps (Figure 6b). The SDII shows smaller changes during this season (Figure 6d), that can be either positive or negative and barely exceeds 10% per century. A general decrease of MWSD is simulated in summer (Figure 6f), especially pronounced over the Southeastern flank of the Alps and in the Po plain, a signal also found in the observations over Switzerland, albeit with a smaller magnitude. Finally, the model shows a general increase in

MNWS (Figure 6h) in summer, which is particularly strong over the Southeastern flank of the Alps. Over Switzerland, this signal is small and not consistent with the observations that show a minor reduction of MNWS. Overall, these results suggest that the decrease of the mean precipitation rates over the Alps in summer is explained by a drastic reduction of WD, with shorter and more frequent wet spells without any strong change of SDII.

4.3 Extreme precipitation

The means and the trends of extreme precipitation rates are described by considering Rx1day seasonally (Figure 7) and annually (Figure 8). Extreme precipitation shows contrasted seasonal and spatial climatological patterns (Figure 7a-c-e-g). In winter and spring, it takes higher values over the Southern Alps (both in France and in Italy) than in the Northern Alps (Figure 7a-c). In summer, extreme values are smaller in the Western Alps than in the Eastern Alps. The most intense events are found in autumn, in both the Western and the Eastern parts of the Southern Alps, with averaged Rx1day ranging between 50 and 70 mm day^{-1} in many areas (Figure 7g). Over Switzerland, the climatological pattern of Rx1day is consistent between the model and the observations, except for some local exceptions. In contrast with the trends of mean precipitation (Figure 4), there is a general increase in Rx1day (Figure 7b-d-f-h) that occurs during the four seasons and both in the plains and in the mountainous areas. The trend in the seasonal Rx1day over the period 1903-2010 takes values between 0 and 40% per century, and generally ranges between 20% and 40% per century over the Alpine mountain range. Such increase in percentages suggests strong changes of local extreme, in particular in the regions where strong events are frequent in autumn (50 to 70 mm day-1, Figure 7g). The magnitude of the change in Rx1day is similar between the model and the observations, but the MeteoSwiss station data show more heterogeneous spatial trends, with some locations where the trends can be small and even slightly negative. The mean increase in Rx1day over the model domain reaches 10%, 10%, 6% and 13% per century, respectively in winter, spring, summer and autumn, confirming a general increase in Rx1day for all the seasons.

The climatological mean of the annual Rx1day (Figure 8a) is dominated by the seasonal Rx1day computed in autumn that shows a similar pattern (Figure 7g). Centennial Rx1day (Figure 8b, maximum Rx1day computed over 1903-2010) shows a pattern similar to the annual average of Rx1day. The strongest centennial events are found in the Southern Alps, in France and Italy, as well as in the Ticino valley in Switzerland, with extreme values locally reaching 250 to 300 mm day^{-1}. The annual trends are inspected in Figure 8c, highlighting a general increase in extreme precipitation. The significance of this trend is described in Figure 8d, where non-significant trends (p-value>0.05) are masked. The annual samples considered here are obviously larger than the seasonal samples, allowing to detect more efficiently significant trends. In that case, a good consistency is found between the model and the MeteoSwiss station, both of them showing only positive trends, ranging between 20 and 40% per century, and covering large parts of the Alps and the Apennines.

4.4 Statistical significance of the trends

The large interannual to decadal variability of the climate in the Europe-North-Atlantic region, in relation with internal climate variability, makes precipitation trends challenging to detect in the Alps. When considering time series over 1971-2008, i.e. a relatively short period, there is no clear tendency of the mean precipitation in the Alps (Figure 3). By computing trends from the beginning of the 20th century, winter increase and summer decrease of mean precipitation emerge from interannual to decadal variability over large areas (Figure 4). Similarly, the positive trends of the annual Rx1day are significant (p-value<0.05) over large areas of the Alps, in particular where the trends are positive and strong (i.e. >10% per century), whereas all the negative and small trends in both the model data at the MeteoSwiss station data are not significant (Figure 8d). Figure 8e illustrates the trend of the annual Rx1day, considering the average of the MeteoSwiss data (purple), the model data averaged over Switzerland (blue) and the whole model domain (red). In agreement with the patterns shown in Figure 8c-d, the mean trend in the annual Rx1day in Figure 8 is positive for both the model outputs and the observations, reaching 9.43, 8.74 and 8.40 mm day^{-1} per century respectively for the MeteoSwiss data, the model over Switzerland and the model over the whole domain. The vertical bars in Figure 8e show the length of the time series required to identify a significant trend over the period 1903-2010, starting from 2010 and going back into the past. Starting from 2010, the trends become significant (p-value<0.05) only when extending backward the time series until 1961, 1932 and 1942 for the MeteoSwiss data, the model integrated over Switzerland and the model integrated over the whole domain respectively, which correspond to length of ~50 to ~80 years. We nonetheless see that shorter time series can lead to significant signals as evidenced in Figure 8f showing the p-value computed to estimate the significant level of the trend. The three curves reach values below 0.05 during the years 1960-1970, highlighting significant trends of Rx1day over 1960-2010 for the observations and over 1970-2010 for the model data.

4.5 Temperature and precipitation relationship

Potential relationship between Rx1day and temperature trends is investigated in this section. On average over the MAR domain, the relationship between the Rx1day anomaly and the annual temperature anomaly is significant (p-value<0.05) and reaches a positive trend by 3.11% $°C^{-1}$ (not shown). This value is smaller than the Clausius-Clapeyron relationship that reaches in theory 6–7%.$°C^{-1}$ (Trenberth et al., 2003). It is also smaller than the value of 7.7%.$°C^{-1}$ reported by Scherrer et al. (2016) using meteorological stations available in Switzerland over the last century. The increase in Rx1day intensity shows a strong spatial variability, with values ranging between 0 and 40% in the MAR simulation (Figure 8a). Also, it occurred during all the seasons (Figure 7), even when the seasonal mean of precipitation is decreasing (Figure 4).

An analysis of the relationship between temperature and strong precipitation is provided in Figure 9 by superposing the areas where the increase of annual Rx1day is positive and significant (Figure 9a) with other variables (hatched areas for Rx1day signal superposed to other variables in Figure 9b-c-d-e-f). The increase in Rx1day intensity is simulated both in areas with a

strong warming (e.g. Apennines) or a moderate one (e.g. over the Alps at high elevation; Figure 9b). The temperature change during the Rx1day is positive and strong in the Apennines in the Western and Northeastern parts of the Italian Alps (up to 4°C century^{-1}) whereas it shows smaller variations in the Northern flank of the Alps, and even negative trends over the Jura (up to -4°C century^{-1}, Figure 9c). Nevertheless, the increase in the Rx1day intensity projects well on the pattern correlation between the Rx1day and the annual temperature (Figure 9d). These findings suggest that warmer temperatures favour strong precipitation events at the annual timescale, but the lack of correlation between the trends in Rx1day and the trends in temperature (Figure 9b) at the local scale demonstrates that other processes than temperature changes affect the Rx1day intensity. One of them is the shift of the seasonality of the occurrence of Rx1day. As shown in Figure 9e, the Rx1day occurs, on average over 1902-2010, from July over the Northern flank of the Alps (day 180 to 210) to August-September (day 210 to 270) over the Southern flank of the Alps. In the Jura, the increase in Rx1day intensity is associated with a Rx1day shift from the summer to the autumn (+30 to +60 days, Figure 9f). This explains the small and even negative centennial trend of temperature during the Rx1day in this area (Figure 9c). Conversely, the strong warming occurring in the Southeastern flank of the Alps and over the Appennine is not associated with any clear change of the seasonality of the Rx1day (Figure 9f). Over Switzerland, Brönnimann et al. (2018) also suggested a shift of the seasonality of the Rx1day. A similar finding is found here, but caution is required with this assumption since the shifts described in Figure 9f are not significant (p-value>0.05). Rx1day positive trends are also simulated in areas with both limited warming and without any shift of the seasonality of the Rx1day occurrence, and in particular in the Alps at high elevation (Figure 9f). This suggests that other processes are probably at play to drive increases in the Rx1day intensity.

5. Discussions and conclusions

Previous work highlighted a temperature increase in the Alps over the last century, associated with an increase in precipitation over the Northern Alps in winter and a drying in summer (Schmidli et al., 2002; Auer et al., 2007; Masson and Frei, 2014; 2016; Brugnara and Maugeri, 2019; Pavan et al., 2019). The detailed features of climate change over the Alps remain however partly unknown, in particular because of the lack of observational data at high elevation, and observational issues with snow precipitation. In addition, the large internal variability of the climate system, especially pronounced in Europe, may overwhelm long-term trends that remain challenging to detect. Here, the MAR model has been used at a 7km resolution over the Alps, over the period 1900-2010 and laterally forced with the ERA-20C reanalysis. A comparison with several datasets (EURO4M, SPAZM, S2M, E-OBS, HISTALP and local MeteoSwiss data) demonstrates that the model is able to reproduce the climatological precipitation rates as well as both the interannual variability and the seasonal cycle of precipitation over the Alps. The high resolution used in the MAR experiment allowed a relatively correct representation of the topography, with a large number of grid cells covering elevation between 2000m and 3500m, corresponding to areas with few available observations. The vertical gradient of precipitation averaged over the Alpine area is estimated to 33% km-1 (1.21 mm day^{-1} km^{-1}) in summer and

38% km-1 (1.15 mm day^{-1} km^{-1}) in winter, with values stronger in the Northern Alps than in the Southern Alps. The spatial variability of this vertical gradient is large, being affected by the local climate conditions.

The seasonal changes of precipitation simulated with MAR are largely related to changes of moisture fluxes found in the ERA-20C reanalysis at the European scale. The model experiment confirms an increase in precipitation during the winter over the North Western Alps, above 500m asl and significant and more pronounced above 1500m asl, with local values of 20% to 30% per century over the period 1903-2010. This increase in precipitation is mainly explained by more intense precipitation during wet days, and it is associated with longer albeit less frequent wet spells, a result consistent with Schmidli and Frei (2005) over Switzerland. The model reproduces the general drying that occurred in summer during the same period, exceeding 40% to 50% per century in the lowlands, whereas it is much smaller (<10% per century) and not significant above 1500m asl. This drying is not related to a decrease of the intensity of precipitation, but it is explained by a drastic reduction of the number of wet days, with shorter and more frequent wet spells. It is consistent with previous work suggesting that the Alpine region appears as an exception in a drying region, where convective precipitation increases locally, in relation to surface warming and sufficient moisture available in the soil at high-elevation areas (Giorgi et al., 2016). The precipitation trends diagnosed over the last decades (i.e. from ~1960) differ from those described from the beginning of the 20th century. In particular, a strong moistening, albeit not significant, is found in autumn over most of the Alpine areas during the last decades and not over the last century. Furthermore, the drying of the Po plain is more pronounced and extended Northward and Westward during the winter, without a clear positive trend of precipitation at high elevation over the last decades during this season. The trends simulated over the last decades are consistent with recent studies based on observations covering the last decades (e.g. Isotta et al., 2014; Pavan et al., 2019).

The model reproduces the observed climatological patterns of the seasonal maximum precipitation, and in particular the large values occurring in the Southern Alps in autumn, exceeding 50 and even 70 mm day^{-1} on average over the period 1903-2010. This result is consistent with the radar observations described in Panziera et al. (2018), showing that annual maximum of daily precipitation rates occur during the autumn whereas the annual maximum of hourly precipitation occur preferentially during the summer in relation with convective events. Centennial daily events reaching 250 to 300 mm day^{-1} are simulated in the Southern Alps, both in France and in Italy, as well as in the Ticino valley. The seasonal maximum of precipitation shows a general increase over the last century and during the four seasons, reaching values between 20% and 40% per century in the Alps. An increase of strong precipitation has been evidenced in previous studies over the European Alps in relation with higher temperature and moisture rates in the atmosphere following the Clausius-Clapeyron relationship (e.g. Ban et al., 2015). A significant relationship between Rx1day intensity and warming is also simulated over the Alps, but with a smaller value reaching 3.11% °C^{-1}. This relationship shows a strong spatial variability in the MAR experiment, suggesting that other processes can affect Rx1day changes.

On one side, the drying of the surface may act as a positive feedback enhancing warming signals, that has been identified as one of the causes of the Mediterreanean amplification (Brogli et al., 2019). On the other side, even with strong warming levels in place, Bronnimann et al. (2018) suggested a limited increase in Rx1day during the summer in the Alps due to moisture limitation. In their study, they pointed out a shift of this index typically observed at the end of the summer toward early summer and early autumn. Albeit not significant, shifts of seasonality of the Rx1day are also found in the MAR experiment, that complexify the relationship between temperature and Rx1day. Nevertheless, the MAR experiment shows an increase of Rx1day both annually and for all seasons, and significant mainly over mountainous areas, a result consistent with the observations from Scherrer et al. (2016) and Brugnara et al. (2019). Further investigations are required to disentangle the different processes driving Rx1day changes, and in particular the moisture availability in both the soil and the atmosphere at different layers. Following Doutreloup et al. (2019) who tested different convective schemes to simulate precipitation with the MAR model, dedicated experiments based on different resolutions, including smaller ones to allow the resolution of convective processes, could help to understand how strong precipitation events are affected by changes in convective precipitation, in particular for strong local events that cannot be simulated with the intermediate resolution used in this study.

In the MAR experiments, the trends of the seasonal maxima of precipitation integrated over the Alps are significant (p-value<0.05) only when considering long time series, typically 50 to 80 years depending on the area considered. Some of these trends are nonetheless significant when computed over recent decades, from the 1960s/1970s to the 2000s. This suggests a recent acceleration of the increase in extreme precipitation, whereas earlier periods with strong precipitation also occurred, in particular during the 1950s/1960s. These ones could be explained by internal climate variability and/or the non-linear response of the climate system to anthropogenic greenhouse gases and aerosols. In particular, the cooling related to aerosol forcing, which peaked during the 1970s/1980s (Koch et al., 2011) over Europe could have masked the warming related to greenhouse gases, and temporarily prevented changes of extreme precipitation. Further model investigations should be conducted to disentangle the variability of the Alpine climate related to internal variability and external forcings. This research is needed to anticipate possibly strong precipitation changes in the Alps under global climate change.

Data availability:

- The MAR model is accessible at https://gitlab.com/Mar-Group, and documented at http://mar.cnrs.fr/
- The outputs of the MAR experiment used in this study can be downloaded at https://doi.org/10.5281/zenodo.3674607
- Alpine Precipitation Grid Dataset (EURO4M-APGD), Version 1, is available on-line at DOI**:**10.18751/Climate/Griddata/APGD/1.0
- ECAD can be downloaded at https://www.ecad.eu//download/ensembles/ensembles.php
- S2M data is available on-line on the AERIS platform at https://doi.org/10.25326/37.
- The SPAZM dataset has been provided by EDF and Météo-France for this research. It could be made available to other researchers under a specific research agreement. Requests should be sent to dtg-demandedonnees-hydro@edf.fr

Author contributions: All authors contributed to design the study. XF, MM and JB ran MAR experiments and produced the figures. MM wrote the manuscript and other authors contributed with suggested changes and comments.

Competing interests: The authors declare no competing interests.

Acknowledgements: As part of the project CDP TRAJECTORIES, this work is funded by the French National Research Agency in the framework of the " Investissements d'avenir" program (ANR-15-IDEX-02). The authors thank the ERASMUS+ program and the VATEX project founded under the program Labex OSUG@2020 (ANR10 LABX56). The author thank the providers of observational datasets: MeteoSwiss, the federal office for meteorology and climatology, for providing the data station over Switzerland as well as the EURO4M-APGD dataset; the HISTALP group (http://www.zamg.ac.at/histalp); Électricité De France (EDF) for providing the SPAZM dataset; the E-OBS dataset from the EU-FP6 project UERRA (http://www.uerra.eu) and the data providers in the ECA&D project (https://www.ecad.eu). The authors thank the "Institut du Développement et des ressources en Informatique" (IDRIS, CNRS, project n°A0080101523) and the GRICAD project (https://gricad.univ-grenoble-alpes.fr/) for providing computer time for the simulations presented in this paper. The figures have been produced with the python package basemap (https://matplotlib.org/basemap/).

Tables:

Index	Unit	Description
TP	mm year-1	Total precipitation amount per year
STP	mm day-1	Total precipitation amount, including wet and dry days, seasonal or annual
WD	days	Number of wet days (≥1mm)
SDII	mm day-1	Simple daily intensity (TP/WD)
Rx1day	mm day-1	Maximum daily precipitation, seasonal or annual
MNWS	no unit	Mean number of wet spells per season
MWSD	days	Mean wet spell duration, averaged over a season (WD/MNWS)

Table 1: Annual and seasonal precipitation indices analysed in this study. Precipitation is the sum of solid and liquid precipitation. These definitions follow the recommendation by the World Meteorological Organization (Peterson et al., 2001; http://etccdi.pacificclimate.org/list_27_indices.shtml).

	Southern Alps (SA)	Northwestern Alps (NWA)	Northeastern Alps (NEA)
MAR - EURO4M	**C=0.89; RMSE=0.46**	**C=0.88; RMSE=0.37**	**0.85; RMSE=0.41**
MAR - SPAZM	**C=0.87; RMSE=0.26**	**C=0.85; RMSE=0.45**	**-**
MAR - E-OBS	**C=0.84; RMSE=0.69**	**C=0.86; RMSE=0.83**	**C=0.79; RMSE=0.90**
MAR - HISTALP	**C=0.02; RMSE=0.64**	**C=-0.10; RMSE=0.73**	**C=-0.22; RMSE=0.66**
EURO4M - SPAZM	C=0.99; RMSE=0.38	C=0.97; RMSE=0.62	-
E-OBS - SPAZM	C=0.93; RMSE=0.63	C=0.95; RMSE=1.14	-
E-OBS - EURO4M	C=0.94; RMSE=0.29	C=0.95; RMSE=0.54	C=0.93; RMSE=0.54
EURO4M - HISTALP	C=0.03; RMSE=0.68	C=-0.08; RMSE=0.74	C=-0.26; RMSE=0.67

Table 2: Correlation Pearson coefficient computed over 1971-2008 (C) and Root Mean Square Error (RMSE) between the time series of precipitation data over 1971-2008 for the three different sub-areas described in Figure 1. All the correlations are significant (p-value>0.05), except those computed with the HISTALP data.

Figures:

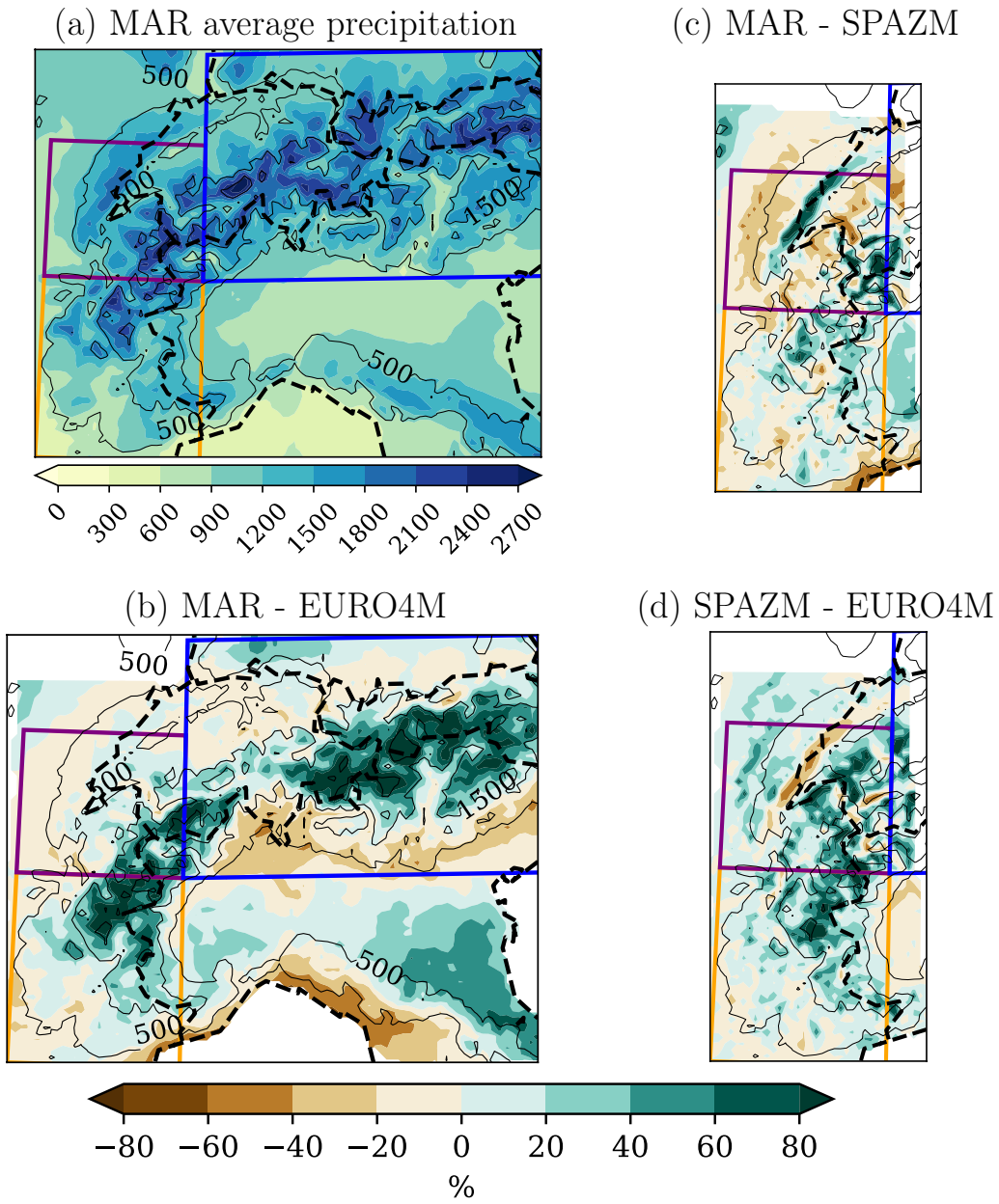

Figure 1: (a) Annual mean of precipitation (TC, mm year^{-1}) over 1971-2008 in the Alps simulated with the model MAR applied with a resolution of 7km and laterally forced with ERA-20C. The colored boxes correspond to the Southern Alps (SA, orange), the Northwestern Alps (NWA, blue) and the Northeastern Alps (NEA, purple). Precipitation differences (%) between: (b) the MAR experiment and the SPAZM dataset, (c) the MAR experiment and the EURO4M-APGD observational gridded datasets, and (d) the SPAZM and the EURO4M-APGD datasets. (c) and (d) are shown only for the area where the SPAZM data is available. The 1000 m-spaced black contours show the topography in the 7km-resolution model, starting from 500 m.asl and political frontiers are denoted with the black dashed lines. The pattern correlation between MAR outputs and observational data is 0.59 and 0.63 respectively with EURO4M and SPAZM (p-value<1e-200).

(a) Annual precip, Southern French Alps

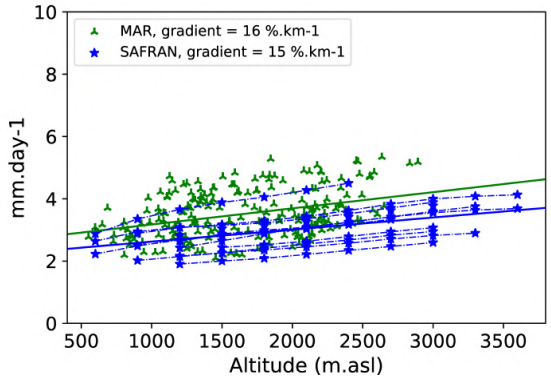

(b) Annual precip, Northern French Alps

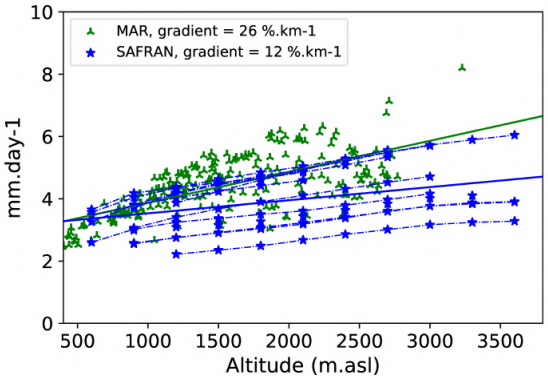

(c) Winter precip, Switzerland

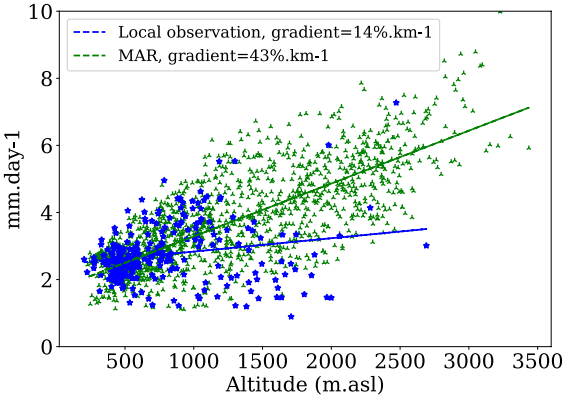

(d) Summer precip, Switzerland

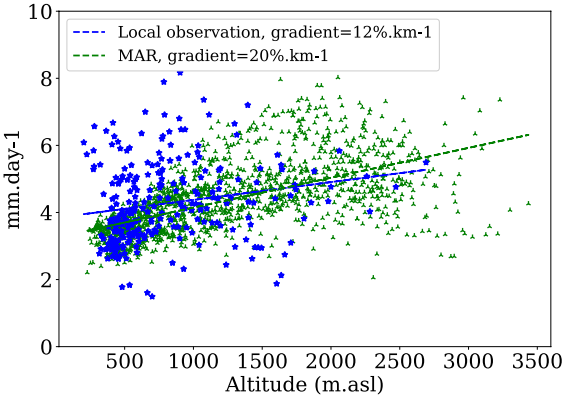

(e) Winter precip, full domain

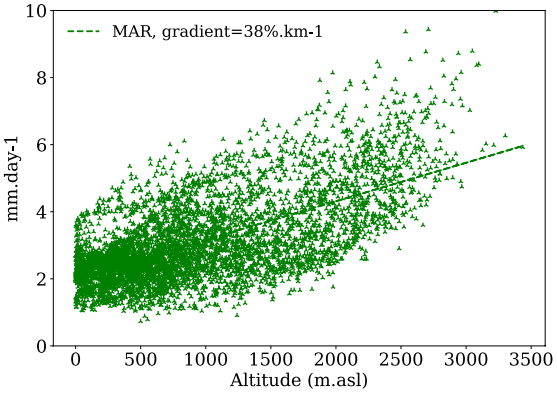

(f) Summer precip, full domain

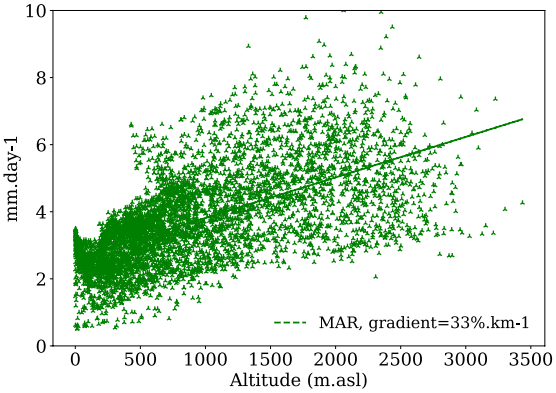

(g) Winter precipitation

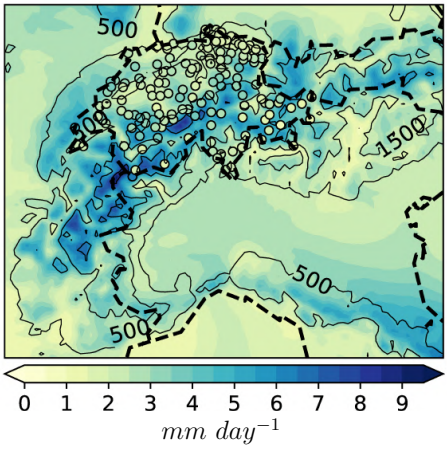

(h) Summer precipitation

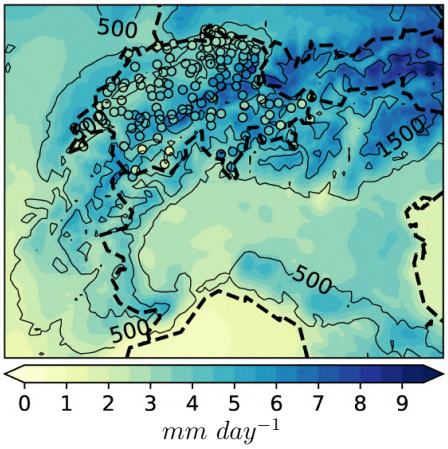

747

Figure 2: Precipitation (STP) averaged over 1971-2008 simulated by MAR and estimated from reanalyses and observations. (a-b-c-d-e-f) show precipitation as a function of the elevation over the Southern (a) and the Northern (b) French Alps in MAR experiments and S2M (SAFRAN) reanalysis, and estimated over Switzerland from local meteorological stations and from the MAR grid cells covering Switzerland during summer (c) and winter (d). The vertical gradient averaged over the whole model domain are shown for winter (e) and summer (f). STP averaged over 1903-2010 in the MAR experiment (shaded, mm day^{-1}) and observed at MeteoSwiss stations in Switzerland (dots, observations available from the beginning of the 20th century) are shown for summer (g) and winter (h). In (g) and (h), the 1000 m-spaced black contours show the topography with a 7km-resolution, starting from 500 m.asl and political frontiers are denoted with the black dahsed lines.

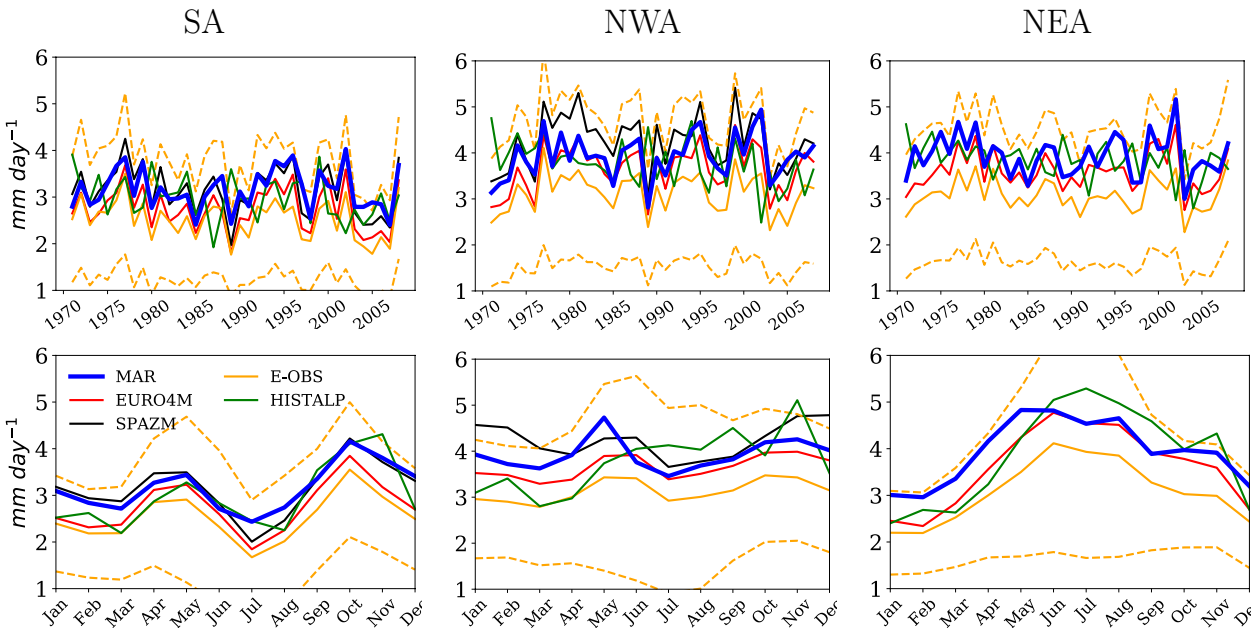

Figure 3: Annual mean precipitation (mm day^{-1}) averaged over the Southern Alps (SA), the Northwestern Alps (NWA) and the Northeastern Alps (NEA) over the period 1971-2008 (top row) and corresponding monthly averaged seasonal cycle over the same period (bottom row). The area covered by the SA, NWA and NEA domains can be visualized in Figure 1. MAR outputs are shown with the observational data sets EURO4M, SPAZM, HISTALP and E-OBS (see text for details). E-OBS (orange solid line) is provided with an estimation of the observational uncertainty (orange dashed lines).

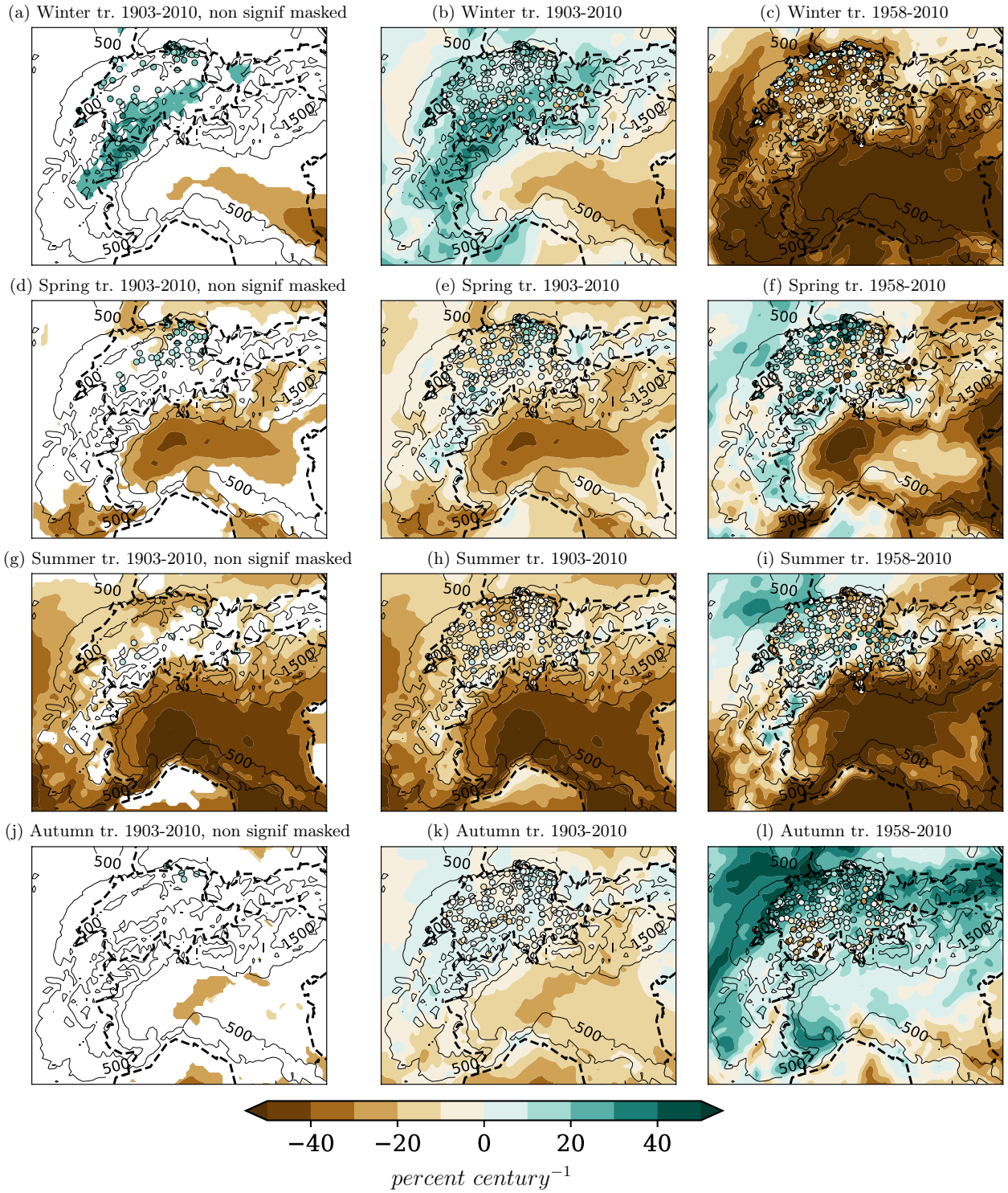

Figure 4: Seasonal linear trends (percent century^{-1}) of precipitation in winter (a-b-c), spring (d-e-f), summer (g-h-i) and autumn (j-k-l), over 1903-2010 for (a-b-d-e-g-h-j-k) and over 1958-2010 for (c-f-i-l). 1000 m-spaced black contours show the topography in the 7km-resolution model, starting from 500 m.asl and frontiers are denoted with the black dashed lines. In (a-d-g-j), the trend is masked when its p-value is below 0.05 (level of confidence lower than 95%; white areas for the model outputs and station data excluded).

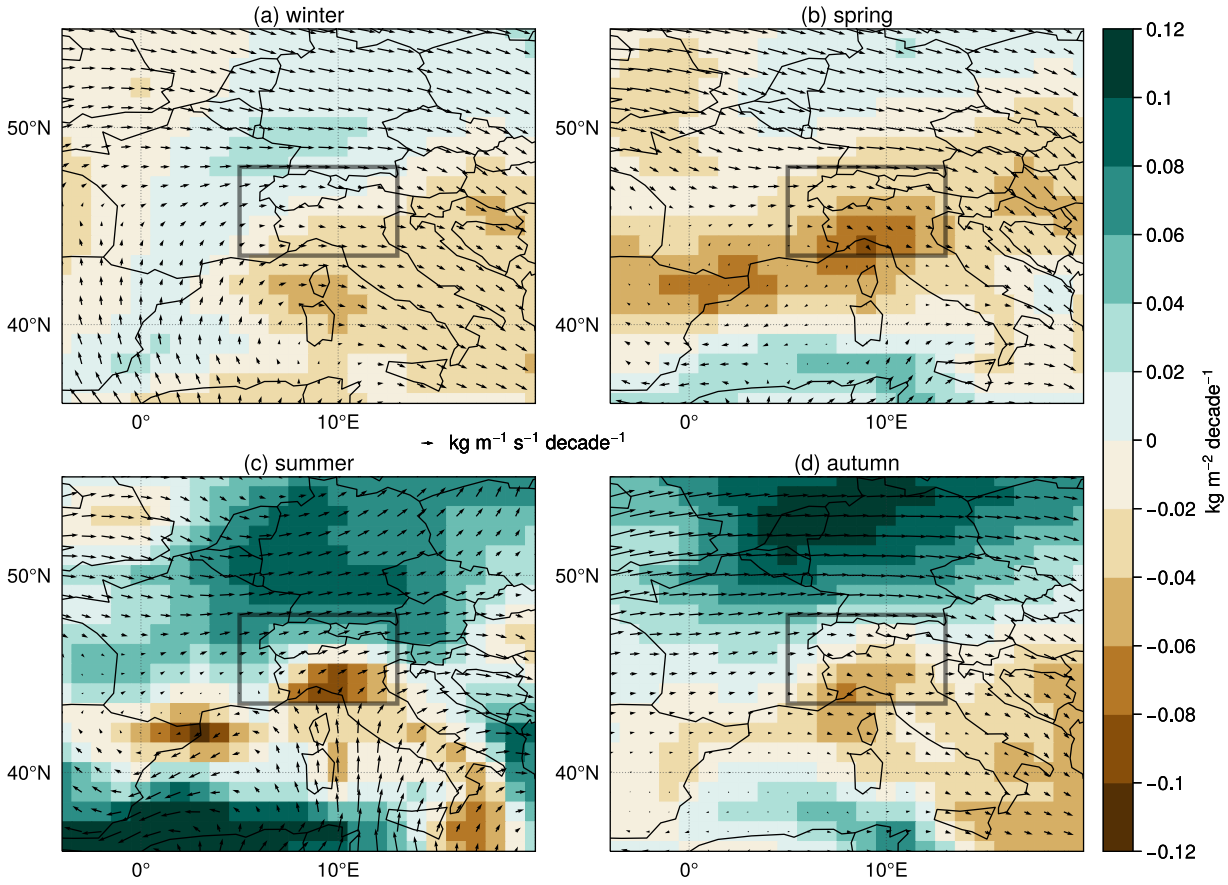

Figure 5: ERA-20C linear trends over 1902-2010 of vertically integrated moisture (shading, kg m^{-2} $decade^{-1}$) and vertically integrated moisture flux (arrows, kg m^{-1} s^{-1} $decade^{-1}$). The rectangle highlights the domain of application of the model MAR.

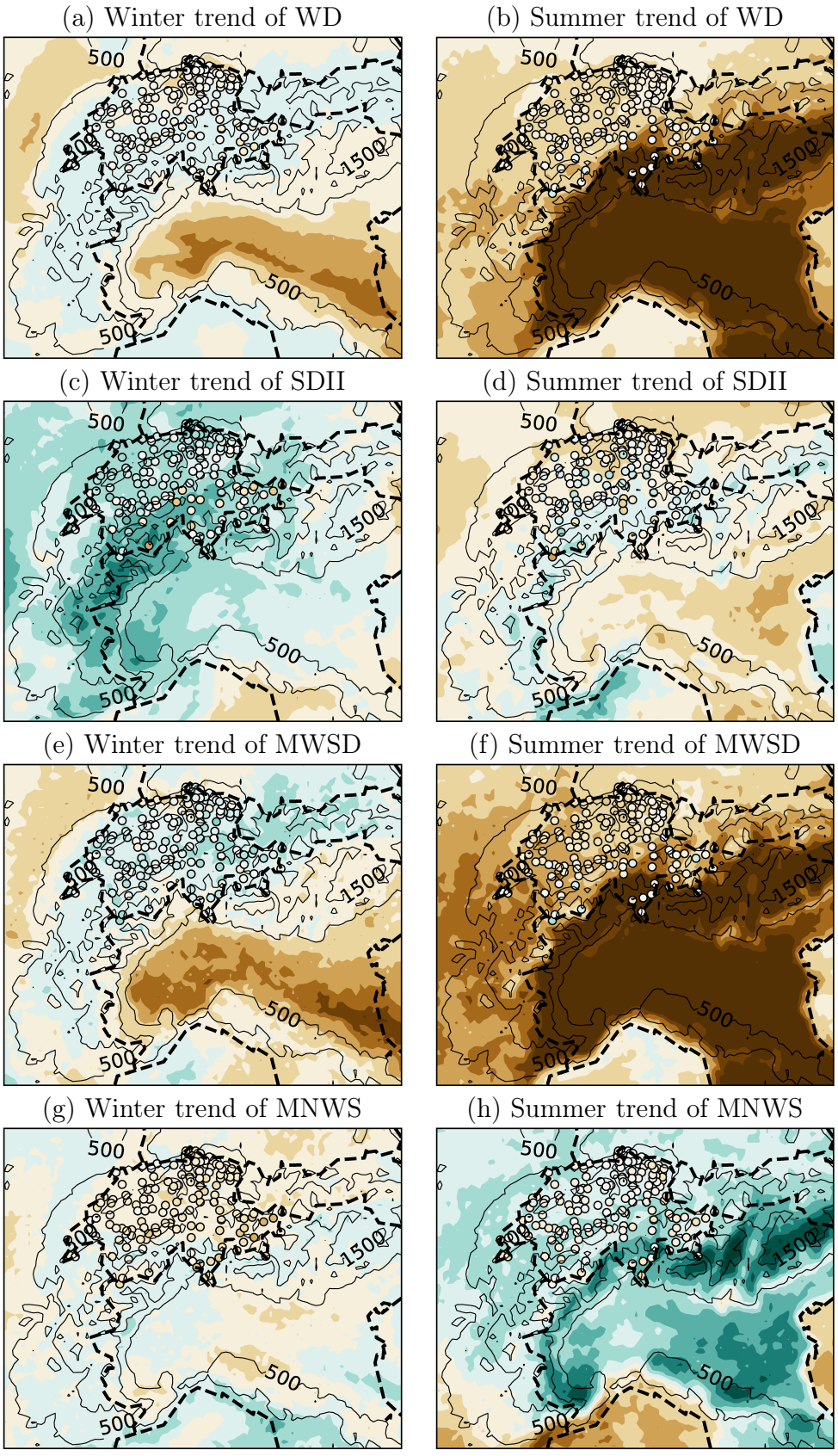
(a) Winter trend of WD
(b) Summer trend of WD
(c) Winter trend of SDII
(d) Summer trend of SDII
(e) Winter trend of MWSD
(f) Summer trend of MWSD
(g) Winter trend of MNWS
(h) Summer trend of MNWS
500
1500
−40
−20
0
20
40
percent century^{-1}

Figure 6: Winter and Summer 1903-2010 trends (percent century^{-1}) of WD (a-b), SDII (c-d), MWSD (e-f) and MNWS (g-h) simulated by the MAR model (shaded) and locally observed in Switzerland (dots). WD is computed as a percentage of the available daily data for observations. Any station from the observational network including missing data is excluded when computing the trends.

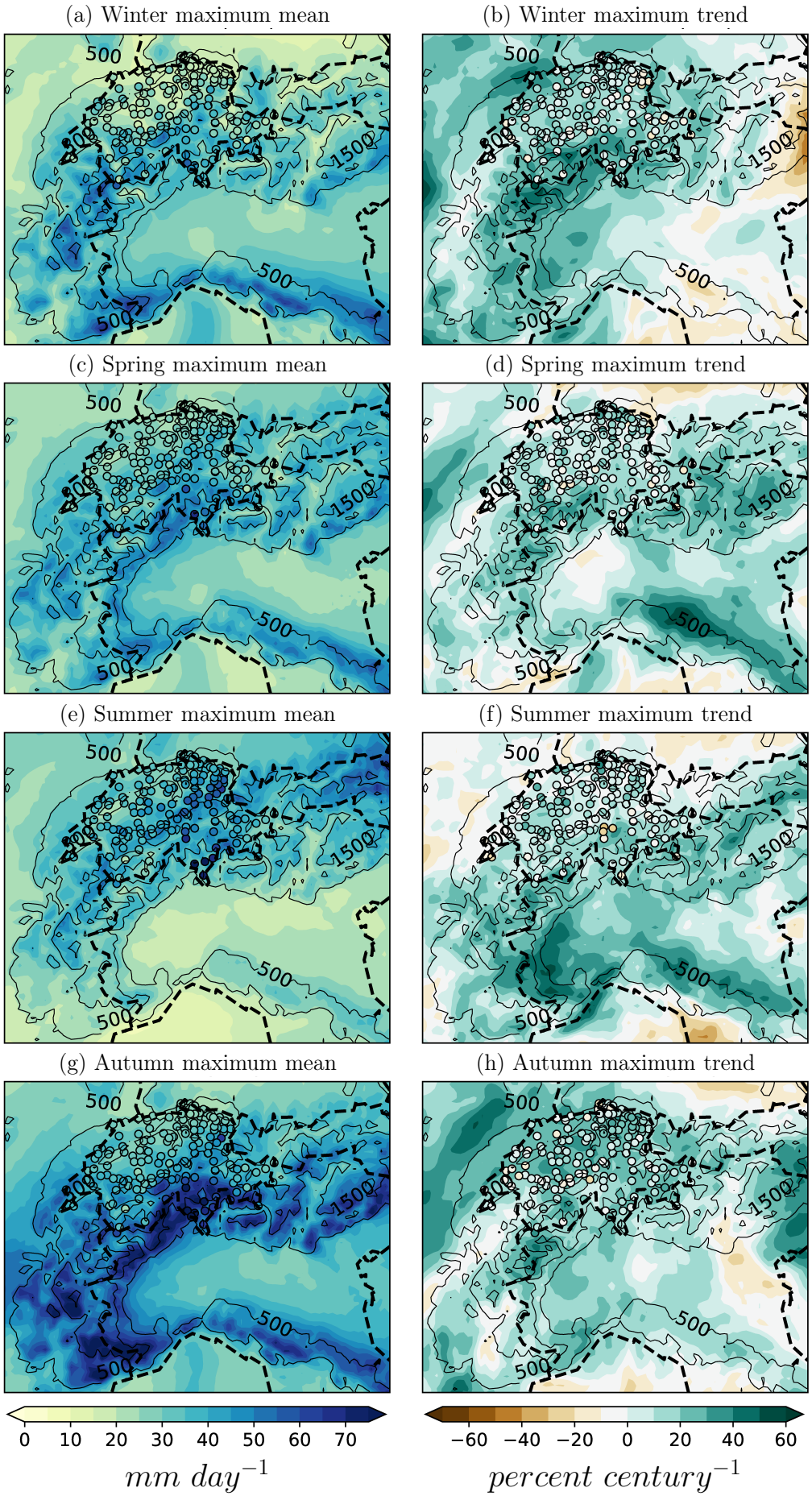
(a) Winter maximum mean
(b) Winter maximum trend
(c) Spring maximum mean
(d) Spring maximum trend
(e) Summer maximum mean
(f) Summer maximum trend
(g) Autumn maximum mean
(h) Autumn maximum trend
500
1000
1500
0 10 20 30 40 50 60 70
mm day^{-1}
−60 −40 −20 0 20 40 60
percent century^{-1}

790 Figure 7: Seasonal mean (mm day^{-1}, left) and trends (percent century^{-1}, right) over the period
791 1903-2010 of the seasonal Rx1day simulated by MAR (shaded) and locally observed in
792 Switzerland (dots) for Winter (a-b), Spring (c-d), Summer (e-f) and Autumn (g-h).
793

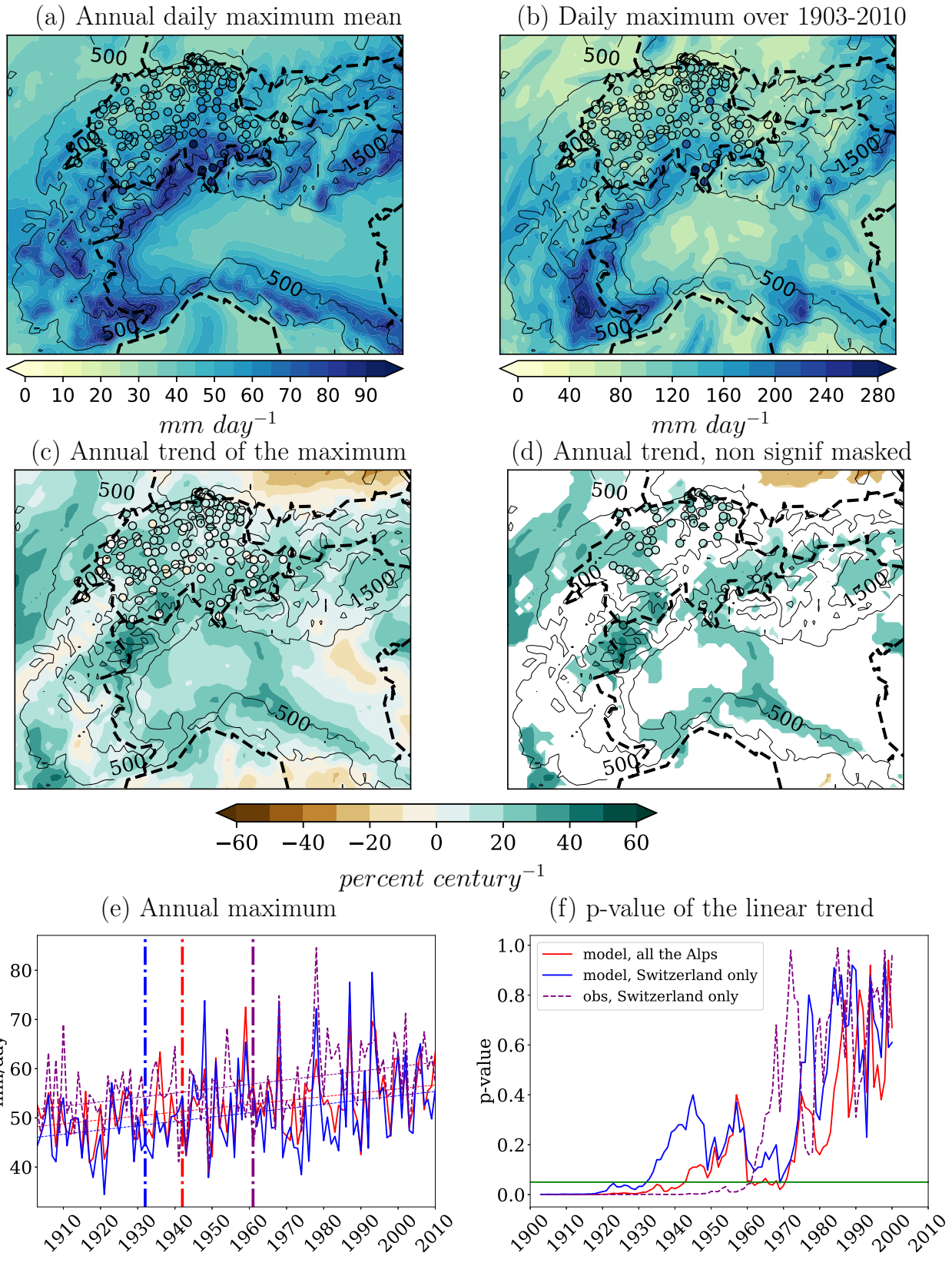
(a) Annual daily maximum mean
500
1000
1500
0 10 20 30 40 50 60 70 80 90
mm day^{-1}
(b) Daily maximum over 1903-2010
0 40 80 120 160 200 240 280
mm day^{-1}
(c) Annual trend of the maximum
(d) Annual trend, non signif masked
−60 −40 −20 0 20 40 60
percent century^{-1}
(e) Annual maximum
mm/day
(f) p-value of the linear trend
p-value
model, all the Alps
model, Switzerland only
obs, Switzerland only

797 Figure 8: Mean (a) and maximum (b) of the annual Rx1day (mm day^{-1}) and its trend (percent
798 century^{-1}) including (c) and excluding (d) the areas where the p-value is lower than 0.05, over
799 1903-2010. Annual Rx1day (e) and associated p-value of the trend (f) over the same period
800 averaged over the model domain (red for the entire Alpine region and blue for the Swiss domain
801 only) and for the MeteoSwiss network (purple, average of the MeteoSwiss data station available
802 over 1903-2010). The vertical bars in (e) highlight the year before which the p-value never
803 exceeds 0.05.

(a) Trend of Rx1day

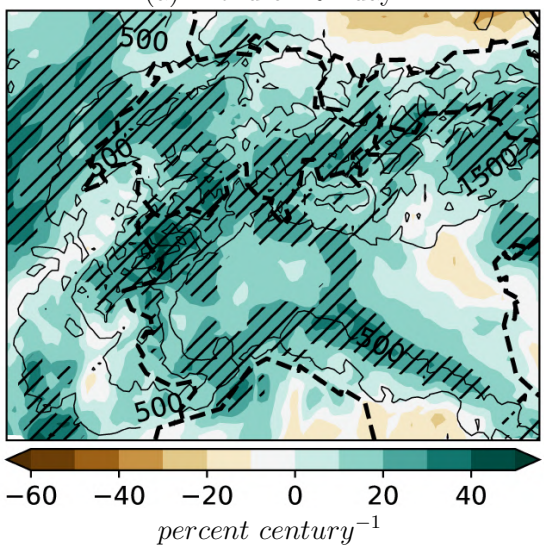

(b) Trend of temperature

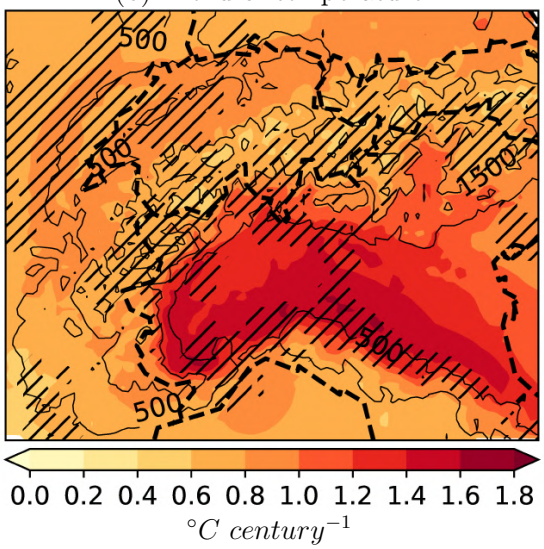

(c) Temperature trend during the Rx1day

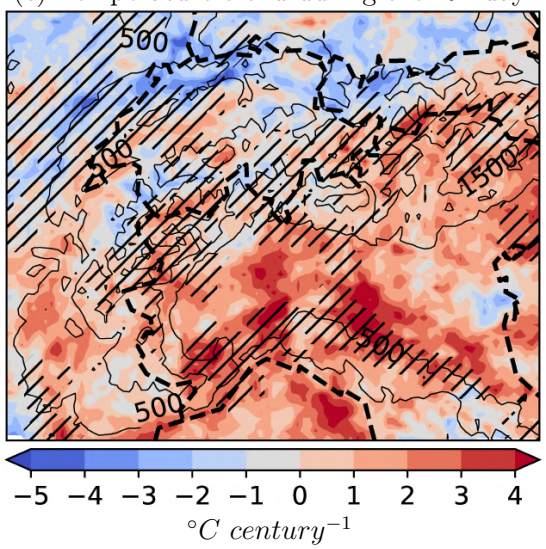

(d) Rx1day correlation with annual temperature

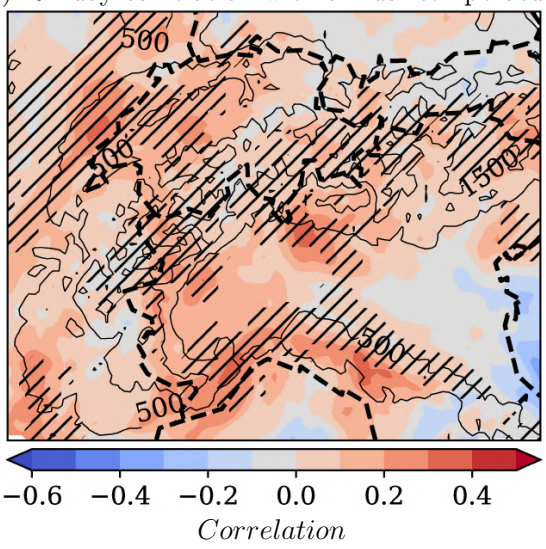

(e) Mean index day of Rx1day

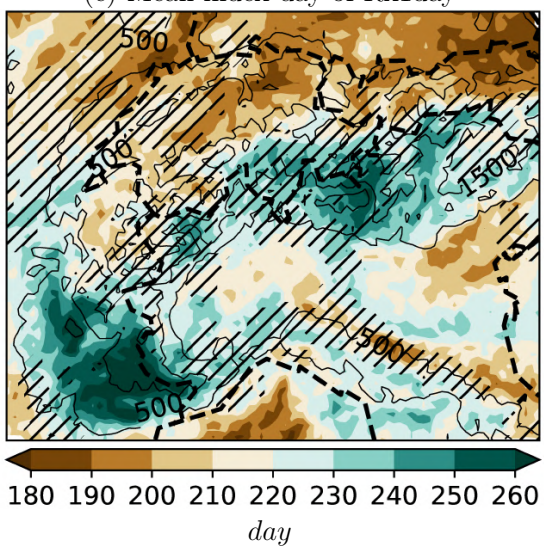

(f) Trend of the index day of Rx1day

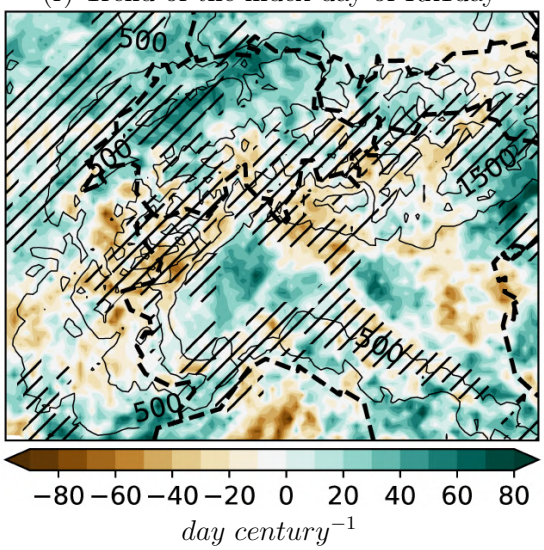

804

Figure 9: Rx1day intensity trend (a), temperature trend (b), temperature trend during the Rx1day occurrence (c) and correlation between Rx1day and annual temperature (d). Mean (e) and trend (f) of the occurrence day of Rx1day over 1903-2010. In all the panels, the hatches highlight the areas where the Rx1day trend is positive and significant (p-value<0.05). Temperature increase and change of the convective versus total precipitation ratio are significant (p-value<0.05) everywhere, whereas the trend (f) of the occurrence day of Rx1 is not significant (p-value>0.05).

References

Agosta, C., Amory, C., Kittel, C., Orsi, A., Favier, V., Gallée, H., van den Broeke, M. R., Lenaerts, J. T. M., van Wessem, J. M., van de Berg, W. J., and Fettweis, X.: Estimation of the Antarctic surface mass balance using the regional climate model MAR (1979–2015) and identification of dominant processes, The Cryosphere, 13, 281–296, https://doi.org/10.5194/tc-13-281-2019, 2019.

Amory, C., Trouvilliez, A., Gallée, H., Favier, V., Naaim-Bouvet, F., Genthon, C., Agosta, C., Piard, L., and Bellot, H.: Comparison between observed and simulated aeolian snow mass fluxes in Adélie Land, East Antarctica, The Cryosphere, 9, 1373–1383, https://doi.org/10.5194/tc-9-1373-2015, 2015.

Auer, I., Böhm, R., Jurkovic, A., Lipa, W., Orlik, A., Potzmann, R., Schöner, W., Ungersböck, M., Matulla, C., Briffa, K. and Jones, P.: HISTALP—historical instrumental climatological surface time series of the Greater Alpine Region. International Journal of Climatology: A Journal of the Royal Meteorological Society, 27(1), pp.17-46, 2007.

Auer, I., and R. Böhm: Combined temperature-precipitation variations in Austria during the instrumental period, Theoretical and applied climatology 49, no. 3 (1994): 161-174, 1994.

Ban, N., J. Schmidli and Schär, C.: Evaluation of the convection-resolving regional climate modeling approach in decade-long simulations, J. Geophys. Res. Atmos, 119, 7889–7907, doi:10.1002/2014JD021478, 2014.

Ban, N., Schmidli, J. and Schär, C.: Heavy precipitation in a changing climate: Does short-term summer precipitation increase faster?. Geophysical Research Letters, 42(4), pp.1165-1172, 2015.

Bartolini, E., Claps, P., and D'Odorico, P.: Interannual variability of winter precipitation in the European Alps: relations with the North Atlantic Oscillation., Hydrol. Earth Syst. Sci., 13, 17–25, https://doi.org/10.5194/hess-13-17-2009, 2009.

Bechtold, P., Basile, E., Guichard, F., Mascart, P., and Richard, E.: A mass flux convection scheme for regional and global models, Q. J. Roy. Meteorol. Soc., 127, 869–886, 2001.

Beniston, M., Farinotti, D., Stoffel, M., Andreassen, L. M., Coppola, E., Eckert, N., Fantini, A., Giacona, F., Hauck, C., Huss, M., Huwald, H., Lehning, M., López-Moreno, J.-I., Magnusson, J., Marty, C., Morán-Tejéda, E., Morin, S., Naaim, M., Provenzale, A., Rabatel, A., Six, D., Stötter, J., Strasser, U., Terzago, S., and Vincent, C.: The European mountain cryosphere: a review of its current state, trends, and future challenges, The Cryosphere, 12, 759–794, https://doi.org/10.5194/tc-12-759-2018, 2018.

Beniston, M.: Mountain weather and climate: a general overview and a focus on climatic change in the Alps. Hydrobiologia, 562(1), pp.3-16, 2006.

Brogli, R., Kröner, N., Sørland, S.L., Lüthi, D. and Schär, C.: The Role of Hadley Circulation and Lapse-Rate Changes for the Future European Summer Climate. Journal of Climate, 32(2), pp.385-404, https://doi.org/10.1175/JCLI-D-18-0431.1, 2019.

Brönnimann, S., Rajczak, J., Fischer, E. M., Raible, C. C., Rohrer, M., and Schär, C.: Changing seasonality of moderate and extreme precipitation events in the Alps, Nat. Hazards Earth Syst. Sci., 18, 2047–2056, https://doi.org/10.5194/nhess-18-2047-2018, 2018.

Brugnara, Y. and Maugeri, M.: Daily precipitation variability in the southern Alps since the late 19th century. International journal of climatology, https://doi.org/10.1002/joc.6034, 2019.

Brunetti, M., Lentini, G., Maugeri, M., Nanni, T., Auer, I., Boehm, R. and Schoener, W.: Climate variability and change in the Greater Alpine Region over the last two centuries based on multi-variable analysis. International Journal of Climatology: A Journal of the Royal Meteorological Society, 29(15), pp.2197-2225, 2009.

Brunetti, M., Maugeri, M., Nanni, T., Auer, I., Böhm, R. and Schöner, W.: Precipitation variability and changes in the greater Alpine region over the 1800–2003 period. Journal of Geophysical Research: Atmospheres, 111(D11), https://doi.org/10.1029/2005JD006674, 2006.

Cornes, R., G. van der Schrier, E.J.M. van den Besselaar, and Jones, P.D.: An Ensemble Version of the E-OBS Temperature and Precipitation Datasets, J. Geophys. Res. Atmos., 123. doi:10.1029/2017JD028200, 2018.

Dee, D.P., Uppala, S.M., Simmons, A.J., Berrisford, P., Poli, P., Kobayashi, S., Andrae, U., Balmaseda, M.A., Balsamo, G., Bauer, D.P. and Bechtold, P.: The ERA-Interim reanalysis: Configuration and performance of the data assimilation system. Quarterly Journal of the royal meteorological society, 137(656), pp.553-597, 2011.

De Ridder, K. and Schayes, G.: The IAGL land surface model, J. Appl. Meteorol., 36, 167–183, 1997.

Doutreloup, S., Wyard, C., Amory, C., Kittel, C., Erpicum, M. and Fettweis, X.: Sensitivity to Convective Schemes on Precipitation Simulated by the Regional Climate Model MAR over Belgium (1987–2017). Atmosphere, 10(1), p.34, 2019.

Douville, H. and Plazzotta, M.: Midlatitude summer drying: An underestimated threat in CMIP5 models?. Geophysical Research Letters, 44(19), pp.9967-9975, 2017

Durand, Y., Laternser, M., Giraud, G., Etchevers, P., Lesaffre, B. and Mérindol, L.: Reanalysis of 44 yr of climate in the French Alps (1958–2002): methodology, model validation, climatology, and trends for air temperature and precipitation. Journal of Applied Meteorology and Climatology, 48(3), pp.429-449, 2009.

Efthymiadis, D., Jones, P.D., Briffa, K.R., Böhm, R. and Maugeri, M.: Influence of large-scale atmospheric circulation on climate variability in the Greater Alpine Region of Europe. Journal of Geophysical Research: Atmospheres, 112(D12), 2007.

Evin G., Wilhelm B., Jenny J.P.: Flood hazard assessment of the Rhône River revisited with reconstructed discharges from lake sediments, Global and Planetary Change 172, 114-123, 2019.

Picouet, C.: Réanalyse de l'équivalent en eau de la couverture neigeuse : développement d'un modèle de neige au pixel. Partie 2 : Structuration d'un modèle neige à l'échelle du pixel au droit des chroniques historiques SWE. Rapport Technique EDF-LTHE-Alcotra, 2012.

Fantini, A., Raffaele, F., Torma, C., Bacer, S., Coppola, E., Giorgi, F., Ahrens, B., Dubois, C., Sanchez, E. and Verdecchia, M.: Assessment of multiple daily precipitation statistics in ERA-Interim driven Med-CORDEX and EURO-CORDEX experiments against high resolution observations. Climate dynamics, 51(3), pp.877-900, 2018.

Fettweis, X., Box, J. E., Agosta, C., Amory, C., Kittel, C., Lang, C., van As, D., Machguth, H., and Gallée, H.: Reconstructions of the 1900–2015 Greenland ice sheet surface mass balance using the regional climate MAR model, The Cryosphere, 11, 1015–1033, https://doi.org/10.5194/tc-11-1015-2017, 2017.

Frei, C., and F. Isotta: Ensemble spatial precipitation analysis from rain gauge data - Methodology and application in theEuropean Alps.J. Geophys. Res. Atmos.,124, 5757–5778,https://doi.org/10.1029/2018JD030004, 2019.

Giorgi, F., Torma, C., Coppola, E., Ban, N., Schär, C. and Somot, S.: Enhanced summer convective rainfall at Alpine high elevations in response to climate warming. Nature Geoscience, 9(8), p.584, 2016.

Giorgi, F. and Lionello, P.: Climate change projections for the Mediterranean region. Global and planetary change, 63(2-3), pp.90-104, 2008.

Gobiet, A., Kotlarski, S., Beniston, M., Heinrich, G., Rajczak, J. and Stoffel, M.: 21st century climate change in the European Alps—a review. Science of the Total Environment, 493, pp.1138-1151, 2014.

Gallée, H., Pettré, P. and Schayes, G.: Sudden cessation of katabatic winds in Adélie Land, Antarctica. Journal of Applied Meteorology, 35(7), pp.1142-1152, 1996.

Gallée, H.: Simulation of the mesocyclonic activity in the Ross Sea, Antarctica, Mon. Weather Rev., 123, 2051–2069, 1995.

Gallée, H. and Schayes, G.: Development of a three-dimensional meso-gamma primitive equation model: katabatic winds simulation in the area of Terra Nova bay, Antarctica, Mon. Weather. Rev., 122, 671–685, 1994.

Gallée, H., Guyomarch, G., and Brun, E.: Impact of snowdrift on the Antarctic ice sheet surface mass balance: possible sensitivity to snow-surface properties, Bound.-Lay. Meteorol., 99, 1–19, 2001.

Gallée, H., Moufouma-Okia, W., Bechtold, P., Brasseur, O., Dupays, I., Marbaix, P., Messager, C., Ramel, R., and Lebel, T.: A high resolution simulation of a West African rainy season using a regional climate model, J. Geophys. Res., 109, D05108, doi:10.1029/2003JD004020, 2004.

Gallée, H., Peyaud, V., and Goodwin. I.: Simulation of the net snow accumulation along the Wilkes Land transect, Antarctica, with a regional climate model, Ann. Glaciol., 41, 17–22, 2005.

Gallée, H., Trouvilliez, A., Agosta, C., Genthon, C., Favier, V. and Naaim-Bouvet, F.: Transport of snow by the wind: A comparison between observations in Adélie Land, Antarctica, and simulations made with the regional climate model MAR. Boundary-layer meteorology, 146(1), pp.133-147, 2013.

Gottardi, F., Obled, C., Gailhard, J. and Paquet, E.: Statistical reanalysis of precipitation fields based on ground network data and weather patterns: Application over French mountains. Journal of hydrology, 432, pp.154-167, 2012.

Gottardi, F.: Estimation statistique et réanalyse des précipitations en montagne Utilisation d'ébauches par types de temps et assimilation de données d'enneigement Application aux grands massifs montagneux français, PhD report, University Joseph Fourier and INPG, https://tel.archives-ouvertes.fr/tel-00419170, 2009.

Gouttevin, I., Turko, M., Branger, F., Leblois, E., Sicart, J.E., Amélioration de la modélisation hydrologique distribuée en conditions naturelles dans les Alpes, Internal report, Action Neige 2016-2017, 2017.

Guillod, B. P., Jones, R. G., Bowery, A., Haustein, K., Massey, N. R., Mitchell, D. M., Otto, F. E. L., Sparrow, S. N., Uhe, P., Wallom, D. C. H., Wilson, S., and Allen, M. R.: weather@home 2: validation of an improved global–regional climate modelling system, Geosci. Model Dev., 10, 1849-1872, https://doi.org/10.5194/gmd-10-1849-2017, 2017.

Hersbach, H. and Dee, D.: ERA5 reanalysis is in production, ECMWF Newsletter 147, ECMWF. Reading, UK, 2016.

Hock, R., G. Rasul, C. Adler, B. Cáceres, S. Gruber, Y. Hirabayashi, M. Jackson, A. Kääb, S. Kang, S. Kutuzov, Al. Milner, U. Molau, S. Morin, B. Orlove, and H. Steltzer, 2019: High Mountain Areas. In : IPCC Special Report on the Ocean and Cryosphere in a Changing Climate [H.-O. Pörtner, D.C. Roberts, V. Masson-Delmotte, P. Zhai, M. Tignor, E. Poloczanska K. Mintenbeck, A. Alegría, M. Nicolai, A. Okem, J. Petzold, B. Rama, N.M. Weyer (eds.)]. http://report.ipcc.ch/srocc/pdf/SROCC_FinalDraft_Chapter2.pdf, 2019.

Hoerling, M., Eischeid, J., Perlwitz, J., Quan, X., Zhang, T. and Pegion, P.: On the increased frequency of Mediterranean drought. Journal of Climate, 25(6), pp.2146-2161, 2012.

Isotta, F.A., Frei, C., Weilguni, V., Perčec Tadić, M., Lassegues, P., Rudolf, B., Pavan, V., Cacciamani, C., Antolini, G., Ratto, S.M. and Munari, M.: The climate of daily precipitation in the Alps: development and analysis of a high-resolution grid dataset from pan-Alpine rain-gauge data. International Journal of Climatology, 34(5), pp.1657-1675, 2014.

Koch, D., Bauer, S.E., Del Genio, A., Faluvegi, G., McConnell, J.R., Menon, S., Miller, R.L., Rind, D., Ruedy, R., Schmidt, G.A. and Shindell, D.: Coupled aerosol-chemistry–climate twentieth-century transient model investigation: trends in short-lived species and climate responses. Journal of Climate, 24(11), pp.2693-2714, 2011.

Kochendorfer, J., Rasmussen, R., Wolff, M., Baker, B., Hall, M. E., Meyers, T., Landolt, S., Jachcik, A., Isaksen, K., Brækkan, R., and Leeper, R.: The quantification and correction of wind-induced precipitation measurement errors, Hydrol. Earth Syst. Sci., 21, 1973-1989, https://doi.org/10.5194/hess-21-1973-2017, 2017.

Kuglitsch, F.G., Toreti, A., Xoplaki, E., Della-Marta, P.M., Zerefos, C.S., Türkeş, M. and Luterbacher, J.: Heat wave changes in the eastern Mediterranean since 1960. Geophysical Research Letters, 37(4), https://doi.org/10.1029/2009GL041841, 2010.

Lüthi, S., Ban, N., Kotlarski, S., Steger, C.R., Jonas, T. and Schär, C.: Projections of Alpine Snow-Cover in a High-Resolution Climate Simulation. Atmosphere, 10(8), p.463, 2019.

Dell'Aquila, A., Mariotti, A., Bastin, S., Calmanti, S., Cavicchia, L., Deque, M., Djurdjevic, V., Dominguez, M., Gaertner, M. and Gualdi, S.: Evaluation of simulated decadal variations over the Euro-Mediterranean region from ENSEMBLES to Med-CORDEX. Climate dynamics, 51(3), pp.857-876, 2018.

Mariotti, A., Pan, Y., Zeng, N. and Alessandri, A.: Long-term climate change in the Mediterranean region in the midst of decadal variability. Climate Dynamics, 44(5-6), pp.1437-1456, 2015.

Masson, D. and Frei, C.: Spatial analysis of precipitation in a high-mountain region: exploring methods with multi-scale topographic predictors and circulation types. Hydrology and Earth System Sciences, 18(11), pp.4543-4563, 2014.

Masson, D. and Frei, C.: Long-term variations and trends of mesoscale precipitation in the Alps: recalculation and update for 1901–2008. International Journal of Climatology, 36(1), pp.492-500, 2016.

Ménégoz, M., Gallée, H., and Jacobi, H. W.: Precipitation and snow cover in the Himalaya : from reanalysis to regional climate simulations, Hydrol. Earth Syst. Sci., 17, 3921-3936, doi:10.5194/hess-17-3921-2013, 2013.

Messager, C., Gallée, H., and Brasseur, O.: Precipitation sensitivity to regional SST in a regional climate simulation during the West African monsoon for two dry years, Clim. Dynam., 22, 249–266, doi:10.1007/s00382-003-0381-x, 2004.

Messager, C., Gallée, H., Brasseur, O., Cappelaere, B., Peugeot, C., Séguis, L., Vauclin, M., Ramel, R., Grasseau, G., Léger, L., Girou, D: Influence of observed and RCM-simulated precipitation on the water discharge over the Sirba basin, Burkina Faso/Niger. Climate Dynamics, 27 (2-3), pp. 199-214, DOI: 10.1007/s00382-006-0131-y, 2006.

992 Molnar, P., Fatichi, S., Gaál, L., Szolgay, J., and Burlando, P.: Storm type effects on super
993 Clausius–Clapeyron scaling of intense rainstorm properties with air temperature, Hydrol. Earth
994 Syst. Sci., 19, 1753–1766, https://doi.org/10.5194/hess-19-1753-2015, 2015.

995 Morcrette, J.-J. Assessment of the ECMWF Model Cloudiness and Surface Radiation Fields at
996 the ARM SGP Site. Mon. Weather Rev. 2002, 130, 257–277.

997 Naithani, J., Gallée, H. and Schayes, G.: Marine air intrusion into the Adelie Land sector of East
998 Antarctica: A study using the regional climate model (MAR). Journal of Geophysical Research:
999 Atmospheres, 107(D11), pp.ACL-6, 2002.

1000 Napoli, A., Crespi, A., Ragone, F., Maugeri, M. and Pasquero, C.: Variability of orographic
1001 enhancement of precipitation in the Alpine region. Scientific reports, 9(1), pp.1-8, 2019.

1002 Panziera, L., Gabella, M., Germann, U., & Martius, O.: A 12-year radar-based climatology of
1003 daily and sub-daily extreme precipitation over the Swiss Alps. International Journal of
1004 Climatology, 38(10), 3749-3769, 2018.

1005 Pavan, V., Antolini, G., Barbiero, R., Berni, N., Brunier, F., Cacciamani, C., Cagnati, A.,
1006 Cazzuli, O., Cicogna, A., De Luigi, C. and Di Carlo, E.: High resolution climate precipitation
1007 analysis for north-central Italy, 1961–2015. Climate dynamics, 52(5-6), pp.3435-3453, 2019.

1008 Peterson, T.C., and Coauthors: Report on the Activities of the Working Group on Climate
1009 Change Detection and Related Rapporteurs 1998-2001,
1010 http://etccdi.pacificclimate.org/list_27_indices.shtml, WMO, Rep. WCDMP-47, WMO-TD
1011 1071, Geneve, Switzerland, 143pp, 2001.

1012 Picouet, C., Réanalyse de l'équivalent en eau de la couverture neigeuse : développement d'un
1013 modèle de neige au pixel. Partie 2 : Structuration d'un modèle neige à l'échelle du pixel au droit
1014 des chroniques historiques SWE. Technical report EDF-LTHE-Alcotra, 2012.

1015 Pieri, A.B., von Hardenberg, J., Parodi, A. and Provenzale, A.: Sensitivity of precipitation
1016 statistics to resolution, microphysics, and convective parameterization: A case study with the
1017 high-resolution WRF climate model over Europe. Journal of Hydrometeorology, 16(4),
1018 pp.1857-1872, 2015.

1019 Poli, P., Hersbach, H., Dee, D.P., Berrisford, P., Simmons, A.J., Vitart, F., Laloyaux, P., Tan,
1020 D.G., Peubey, C., Thépaut, J.N. and Trémolet, Y.: ERA-20C: An atmospheric reanalysis of the
1021 twentieth century. Journal of Climate, 29(11), pp.4083-4097, 2016.

1022 Qasmi, S., Cassou, C., & Boé, J.: Teleconnection between Atlantic multidecadal variability and
1023 European temperature: Diversity and evaluation of the Coupled Model Intercomparison Project
1024 phase 5 models. Geophysical Research Letters, 44(21), 11-140, 2017.

1025 Raymond F., Wilhelm B., Anquetin S.: Is Precipitation the Main Trigger of Medium- Magnitude
1026 Floods in Large Alpine Catchments?, Water 11, 2507, 2019.

Rottler, E., Kormann, C., Francke, T., et al. : Elevation-dependent warming in the Swiss Alps 1981–2017: Features, forcings and feedbacks. International Journal of Climatology, vol. 39, no 5, p. 2556-2568, 2019.

Scherrer, S.C., Fischer, E.M., Posselt, R., Liniger, M.A., Croci-Maspoli, M. and Knutti, R.: Emerging trends in heavy precipitation and hot temperature extremes in Switzerland. Journal of Geophysical Research: Atmospheres, 121(6), pp.2626-2637, 2016.

Schmidli, J., Schmutz, C., Frei, C., Wanner, H. and Schär, C.: Mesoscale precipitation variability in the region of the European Alps during the 20th century. International Journal of Climatology: A Journal of the Royal Meteorological Society, 22(9), pp.1049-1074, 2002.

Schmidli, J. and Frei, C.: Trends of heavy precipitation and wet and dry spells in Switzerland during the 20th century. International Journal of Climatology: A Journal of the Royal Meteorological Society, 25(6), pp.753-771, 2005.

Smiatek, G., Kunstmann, H. and Senatore, A.: EURO-CORDEX regional climate model analysis for the Greater Alpine Region: Performance and expected future change. Journal of Geophysical Research: Atmospheres, 121(13), pp.7710-7728, 2016.

Steger, C., Kotlarski, S., Jonas, T., and Schär, C.: Alpine snow cover in a changing climate: A regional climate model perspective,Clim. Dynam., 41, 735–754, 2013

Torma, C., Giorgi, F. and Coppola, E.: Added value of regional climate modeling over areas characterized by complex terrain—Precipitation over the Alps. Journal of Geophysical Research: Atmospheres, 120(9), pp.3957-3972, 2015.

Trenberth, K.E., Dai, A., Rasmussen, R.M. and Parsons, D.B.: The changing character of precipitation. Bulletin of the American Meteorological Society, 84(9), pp.1205-1218, 2003.

Uppala, S.M., Kållberg, P.W., Simmons, A.J., Andrae, U., Bechtold, V.D.C., Fiorino, M., Gibson, J.K., Haseler, J., Hernandez, A., Kelly, G.A. and Li, X.: The ERA-40 re-analysis. Quarterly Journal of the Royal Meteorological Society: A journal of the atmospheric sciences, applied meteorology and physical oceanography, 131(612), pp.2961-3012, 2005.

Van den Besselaar, E.J., Haylock, M.R., Van der Schrier, G. and Klein Tank, A.M.G.: A European daily high-resolution observational gridded data set of sea level pressure. Journal of Geophysical Research: Atmospheres, 116(D11), 2011.

Verfaillie, D., Favier, V., Gallée, H., Fettweis, X, Agosta, C., Jomelli, V. Regional modeling of surface mass balance on the Cook Ice Cap, Kerguelen Islands, Climate Dynamics, DOI: 10.1007/s00382-019-04904-z., 2019.

Vernay, M., Lafaysse, M., Hagenmuller , P., Nheili , R., Verfaillie , D., & Morin , S. The S2M meteorological and snow cover reanalysis in the French mountainous areas (1958 - present) [Data set]. AERIS. https://doi.org/10.25326/37, 2019.

1062 Vionnet, V., Six, D., Auger, L., Dumont, M., Lafaysse, M., Quéno, L., Réveillet, M.,
1063 Dombrowski Etchevers, I., Thibert, E. and Vincent, C., Sub-kilometer precipitation datasets for
1064 snowpack and glacier modeling in alpine terrain, Frontiers in Earth Science, 7, p.182., 2019.

1065 Viviroli, D. and Weingartner, R.: "Water towers"—A global view of the hydrological
1066 importance of mountains. In Mountains: sources of water, sources of knowledge (pp. 15-20).
1067 Springer, Dordrecht, 2008.

1068 Viviroli, D., Kummu, M., Meybeck, M. and Wada, Y.: Increasing dependence of lowland
1069 population on mountain water resources, https://eartharxiv.org/fr5uj, 2019.

1070 Wanner, H., Rickli, R., Salvisberg, E., Schmutz, C. and Schüepp, M.: Global climate change and
1071 variability and its influence on alpine climate—concepts and observations. Theoretical and
1072 Applied Climatology, 58(3-4), pp.221-243, 1997.

1073 Wyard, C., Doutreloup, S., Belleflamme, A., Wild, M. and Fettweis, X.: Global Radiative Flux
1074 and Cloudiness Variability for the Period 1959–2010 in Belgium: A Comparison between
1075 Reanalyses and the Regional Climate Model MAR. Atmosphere, 9(7), p.262, 2018.

1076 Wyard, C., Scholzen, C., Fettweis, X., Van Campenhout, J. and François, L., 2017. Decrease in
1077 climatic conditions favouring floods in the south-east of Belgium over 1959–2010 using the
1078 regional climate model MAR. International Journal of Climatology, 37(5), pp.2782-2796, 2017.

1079 Zubler, E.M., Fischer, A.M., Fröb, F. and Liniger, M.A.: Climate change signals of CMIP5
1080 general circulation models over the Alps–impact of model selection. International Journal of
1081 Climatology, 36(8), pp.3088-3104, 2016.

Appendix

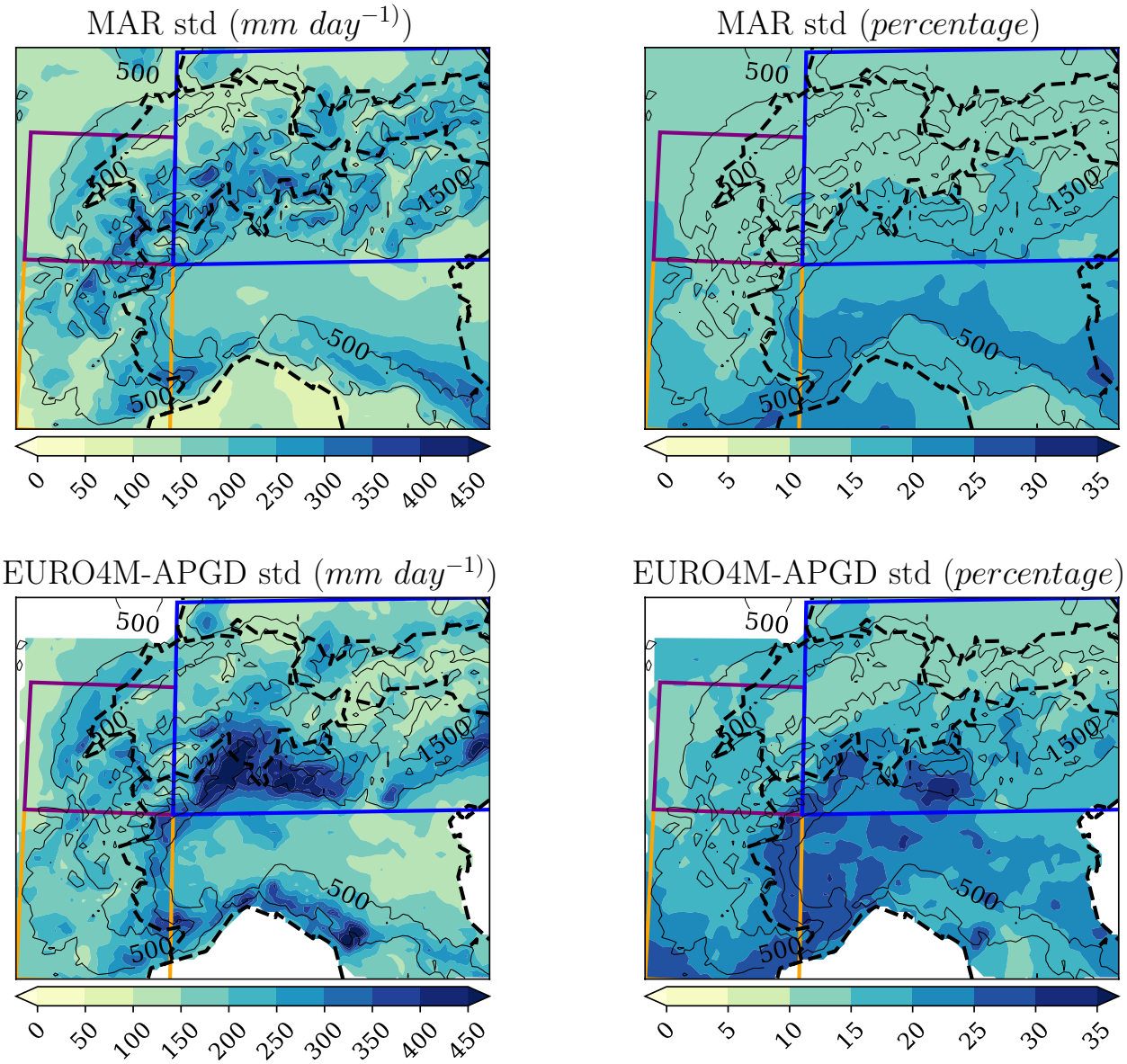

Figure A1: Standard deviation of annual precipitation over 1971-2008, in mm day-1 (left) and in percent (right), in the MAR experiment (top) and in the EURO4M-APGD dataset (bottom).